Title:

RdDM mutants reduce histone methylation rather than DNA methylation at the paramutated maize *b1* enhancer

Authors:

Iris Hövel[1], Rechien Bader[1], Marieke Louwers[1,2], Max Haring[1,3], Kevin Peek[1], Jonathan I. Gent[4] and Maike Stam[1]

Author Affiliations:

[1] Swammerdam Institute for Life Sciences, Universiteit van Amsterdam, P.O. box 1210, 1090 GE Amsterdam, The Netherlands.

[2] argenx BV, Industriepark Zwijnaarde 7, 9052 Zwijnaarde (Ghent), Belgium

[3] Universiteit van Amsterdam, P.O. box 19185, 1000 GD Amsterdam, The Netherlands.

[4] Department of Plant Biology, University of Georgia, Athens, Georgia 30602, USA.

Corresponding Author:

m.e.stam@uva.nl (e-mail), +31-20-5257655 (phone)

The author responsible for distribution of materials integral to the findings presented in this article in accordance with the policy described in the Instructions for Authors (https://academic.oup.com/plphys/pages/general-instructions) is: Maike Stam.

Short Running head:

Silencing release without DNA methylation loss

Abstract

Paramutation is the transfer of mitotically and meiotically heritable silencing information between two alleles. With paramutation at the maize *booster1* (*b1*) locus, the low expressed *B'* epiallele heritably changes the high expressed *B-I* epiallele into *B'* with 100% frequency. This requires specific tandem repeats and multiple components of the RNA-directed DNA methylation (RdDM) pathway, including the RNA-dependent RNA polymerase (RdRP, *mediator of paramutation1*, MOP1), the second-largest subunit of RNA polymerase IV and V (NRP(D/E)2a, *mediator of paramutation2,* MOP2), and the largest subunit of RNA Polymerase IV (NRPD1, *mediator of paramutation3*, MOP3). Mutations in *mop* genes prevent paramutation and release silencing at the *B'* epiallele. In this study we investigated the effect of mutations in *mop1*, *mop2* and *mop3* on chromatin structure and DNA methylation at the *B'* epiallele, and especially the regulatory hepta-repeat 100 kb upstream of the *b1* gene.

We show that mutations in *mop1* and *mop3* result in decreased repressive histone modifications H3K9me2 and H3K27me2 at the hepta-repeat. Associated with this decrease are partial activation of the hepta-repeat enhancer function, formation of a multi-loop structure, and elevated *b1* expression. In *mop2* mutants, which do not show elevated *b1* expression, H3K9me2 and H3K27me2 and a single-loop structure like in wild type *B'* are retained. Surprisingly, high DNA methylation levels at the *B'* hepta-repeat remains in all three mutants. Our results raise the possibility of MOP factors mediating RNA-directed histone methylation rather than RNA-directed DNA methylation at the *b1* locus.

53 **Introduction**

54 Paramutation involves meiotically heritable epigenetic changes in gene expression caused by
55 *trans*-communication between homologous alleles (Hövel et al., 2015; Hollick, 2017;
56 Springer and McGinnis, 2015; Ronsseray, 2015). Paramutation has been studied in plants,
57 such as maize and tomato, but also in animals, such as mice, Drosophila and *C. elegans*. In
58 maize, paramutation has been best studied at genes encoding transcriptional regulators of the
59 flavonoid pigmentation pathway, *r1 (red1)*, *b1* (*booster1)*, *pl1 (plant color1)*, and *p1*
60 (*pericarp color1*). Most alleles of these genes do not participate in paramutation; they are
61 neutral to paramutation; only specific alleles do. The ability to participate in paramutation is
62 often dependent on repeated sequences (for reviews see Hövel et al., 2015; Hollick, 2017).
63 The alleles participating in paramutation at the *b1* locus are *B′* and *B-I*. *B′* and *B-I* have the
64 same DNA sequence; they are epialleles (Stam et al., 2002a). *B′* is the paramutated, inactive
65 state of *b1* (light pigmented plant), and *B-I* the paramutable, active state of *b1* (dark
66 pigmented plant). In a *B'/B-I* heterozygote, the low expressed *B'* epiallele is paramutagenic;
67 it changes the high expressed *B-I* epiallele into *B'* with 100% efficiency, reducing the *B-I*
68 transcription rate 10-20 fold (Patterson et al., 1993). The change of *B-I* into *B'* is mitotically
69 and meiotically heritable and requires multiple tandem copies of part of an 853-nt sequence
70 located ~100 kb upstream of the *b1* transcription start site (TSS) (Stam et al., 2002a; Stam et
71 al., 2002b; Belele et al., 2013). *B-I* and *B'* carry seven copies of the 853-nt sequence (hepta-
72 repeat), while *b1* alleles insensitive (neutral) to paramutation carry one copy of the repeat
73 unit. Our previous study implicated DNA hypermethylation at the hepta-repeat in both the
74 maintenance and establishment of silencing at the *b1* hepta-repeat, while the presence of
75 Histone H3 lysine K27 dimethylation (H3K27me2) at the hepta-repeat and *b1* coding region
76 was associated with the maintenance of the silenced *B'* state (Haring et al., 2010). Besides
77 their role in paramutation, the 853-nt tandem repeats carry transcriptional enhancer
78 sequences that are required for tissue-specific enhancement of *b1* expression (Belele et al.,
79 2013; Louwers et al., 2009a). In *B-I*, tissue-specific activation of *b1* expression in husk tissue
80 is associated with H3 acetylation (at K9 and K14) and nucleosome depletion at the hepta-
81 repeat (Haring et al., 2010). High *b1* expression levels are in addition associated with
82 chromosomal interactions between the hepta-repeat, TSS and other regulatory regions at the
83 *b1* locus, ~15, ~47 and ~107 kb upstream of the TSS (Louwers et al., 2009a). In *B'*,
84 chromosomal interactions with the TSS, but not with the ~15, ~47 and ~107 kb regions were
85 observed.

86 To this date, several genes, called *mediator of paramutation* (*mop*) and *required to*

87 *maintain repression (rmr)*, have been identified to be required to establish paramutation at
88 multiple maize loci (*b1, pl1, r1, p1*) (Dorweiler et al., 2000; Hollick et al., 2005; Sidorenko et
89 al., 2009; Sidorenko and Chandler, 2008; Sloan et al., 2014; Stonaker et al., 2009). In mutants
90 of these genes, the paramutagenic alleles can no longer silence the expression of paramutable
91 alleles. The *mop1* and *rmr* genes identified to play such role in maize share homology with
92 genes involved in the RNA-directed DNA methylation (RdDM) pathway in *Arabidopsis*
93 *thaliana*. This pathway induces *de novo* DNA methylation (5mC) in all sequence contexts
94 (CG, CHG and CHH, where H is an A, T, or C) at transposable elements and selected genes
95 (Matzke and Mosher, 2014; Rymen et al., 2020; Zemach et al., 2013). In the RdDM pathway,
96 plant-specific RNA Polymerase IV (Pol IV) transcripts are converted into double-stranded
97 RNA by RNA-DEPENDENT RNA POLYMERASE 2 (RDR2), and processed into 24-nt
98 small interfering RNAs (siRNAs) by DICER-LIKE 3 (DCL3). One strand of the siRNAs is
99 incorporated into a complex containing ARGONAUTE 4 (AGO4), targeting the resulting
100 complex to complementary transcripts generated by RNA Polymerase V (Pol V).
101 Subsequently, DOMAINS REARRANGED METHYLTRANSFERASE2 (DRM2) is
102 recruited, mediating *de novo* DNA methylation of cytosines in all sequence contexts (CG,
103 CHG and CHH; H = A, T or C). This in turn leads to recruitment of histone modifying
104 enzymes and chromomethyltransferases such as CROMOMETHYLASE 3 (CMT3), which
105 methylates DNA in the CHG context. It also leads to recruitment of the replication-coupled
106 DNA methyltransferase MET1, which methylates in the CG context.
107 The first gene identified to be required for the establishment of paramutation was
108 *mop1*, encoding a putative ortholog of RDR2 in Arabidopsis (Alleman et al., 2006; Dorweiler
109 et al., 2000; Haag et al., 2014; Woodhouse et al., 2006a). Subsequently *mop2/rmr7* and
110 *mop3/rmr6* were identified (Erhard et al., 2009; Haag et al., 2014; Hollick et al., 2005;
111 Sidorenko et al., 2009; Sloan et al., 2014; Stonaker et al., 2009); *mop2/rmr7* encodes the
112 maize ortholog of NRP(D/E)2a, the second largest subunit of Pol IV (NRPD1) and Pol V
113 (NRPE1), while *mop3/rmr6*, encodes NRPD1, the largest subunit of Pol IV. Mutations in
114 *mop1*, *mop2/rmr7* and *rmr6* have been shown to cause a severe decrease in the global 24-nt
115 siRNA levels, which is in line with their expected function in the RdDM pathway (Erhard et
116 al., 2009; Jia et al., 2009; Nobuta et al., 2008; Sidorenko et al., 2009; Stonaker et al., 2009). In
117 addition, for *mop1-1* and *mop2-1* mutants, diminished siRNAs levels at the *b1* hepta-repeat
118 were shown (Arteaga-Vazquez et al., 2010; Sidorenko et al., 2009). The nature of the
119 contribution of RdDM is, however, still unclear. The *b1* repeats are transcribed and yield
120 siRNAs not only from *B'*, but also *B-I* and a neutral *b1* allele, suggesting that presence of

121 siRNAs is not sufficient for paramutation (Alleman et al., 2006; Arteaga-Vazquez et al.,
122 2010; Sidorenko et al., 2009).

123 In line with a role for RdDM, *mop1*, *mop2* and *mop3* mutations are shown to induce a
124 reduction in DNA methylation at specific transposons, especially at DNA sequence regions
125 with high levels of DNA methylation in a CHH context, also called mCHH islands (Gent et
126 al., 2014, 2013; Li et al., 2015, 2014). This reduction in DNA methylation at mCHH islands
127 was indicated to occur in all cytosine contexts and was strongest in *mop3* and weakest in
128 *mop2* mutants. Decreased DNA methylation levels were associated with increased expression
129 of several transposons (Jia et al., 2009; Li et al., 2015; Woodhouse et al., 2006b).

130 The *mop1*, *mop2/rmr7* and *mop3/rmr6* gene products are not only necessary for
131 paramutation, they are also reported to be required to maintain the silent state of *B′* and *Pl′*,
132 the paramutagenic *b1* and *pl1* loci (Dorweiler et al., 2000; Hollick et al., 2005; Sidorenko et
133 al., 2009; Sloan et al., 2014; Stonaker et al., 2009). In these mutants, increased expression
134 and/or plant pigmentation was observed. Upon crossing out the mutations, depending on the
135 gene and the mutation studied, the epialleles either lose expression and become
136 paramutagenic again or retain expression and are indistinguishable from their non-
137 paramutated states. The first is true for *B′; B'* does not revert to *B-I* in any of the three mutants
138 (Dorweiler et al., 2000) Similarly, *Pl′* does not revert to the active *Pl-Rh* state in *rmr7* mutants
139 (Stonaker et al., 2009). Thus, the epigenetic memory of *B′* and *Pl′* persists in mutants in spite
140 of increased epiallele expression. In *rmr6* mutants, however, the epigenetic memory of *Pl′* can
141 be erased: *Pl′* can stably revert to *Pl-Rh* in *rmr6* mutants (Hollick et al., 2005).

142 To get a better understanding of the role of the *mop* genes in the maintenance of *B′*
143 silencing, more specifically their role in the maintenance of DNA methylation and repressive
144 histone modifications, we examined the effect of *mop1*, *mop2* and *mop3* mutants on
145 chromatin structure and DNA methylation at the *B'* epiallele, and especially the regulatory
146 hepta-repeat 100 kb upstream of the *b1* coding sequence. Surprisingly, our results show that
147 none of the three *mop* genes is required to maintain high DNA methylation levels at the *B′*
148 hepta-repeat. High DNA methylation levels are maintained in all three mutants. In *mop2*
149 mutants, the *B′* epiallele in addition remains low expressed and retains high levels of the
150 repressive histone modifications H3K9me2 and H3K27me2. The elevated *b1* expression
151 levels in *mop1* and *mop3* mutants are, however, associated with significant reductions in
152 H3K9me2 and H3K27me2 at the hepta-repeat. We propose that this decrease in repressive
153 histone modifications allows the activation of the hepta-repeat enhancer function despite the
154 high DNA methylation levels. Our results indicate that MOP1 and MOP3 play a role in

155 maintaining H3K9me2 and H3K27me2 independent of a role in establishing DNA
156 methylation.
157
158 **Results**
159
160 **Approach**
161 To disentangle the effect of the *mop1-1, mop2-1, mop2-2* and *mop3-1* mutations (Alleman et
162 al., 2006; Dorweiler et al., 2000; Li et al., 2015; Sidorenko et al., 2009; Sloan et al., 2014) on
163 the epigenetic marks and chromatin features that define the mitotically and meiotically
164 heritable *B'* state from the effect on tissue-specific activation of *B'* expression, where
165 relevant, experiments were performed on two types of tissues: seedling and husk tissue. In
166 seedling tissue, comprising 1-month old seedlings with the exposed leaf blades and roots
167 removed, *B'* as well as *B-I* are very low expressed (Haring et al., 2010). In husk tissue (the
168 leaves surrounding the ear) expression of *b1* is transcriptionally activated, resulting in high *B-*
169 *I* and low *B'* expression. *B'* in a wild-type background was compared to *B'* in *mop* mutant
170 backgrounds. Plants carrying the *B-I* allele served as a positive control for an active *b1*
171 epiallele. The *mop1-1, mop2-2* and *mop3-1* mutations act recessive in preventing
172 paramutation between *B'* and *B-I*, and in their effect on pigmentation (Dorweiler et al., 2000;
173 Sidorenko et al., 2009; Sloan et al., 2014), therefore for these mutants only homozygous
174 mutant tissues were used in our analyses. The *mop2-1* mutation acts dominant in preventing
175 paramutation, and was reported to act recessive for enhancing pigmentation (Sidorenko et al.,
176 2009). Tissues of both heterozygous *Mop2/mop2-1,* and homozygous *mop2-1* mutants were
177 used in our analyses. In the text individuals homozygous for *B'* and a *mop* mutation are
178 referred to as *B' mop1-1, B' mop2-1, B' mop2-2,* and *B' mop3-1. Mop2 B'/mop2-1 B'*
179 individuals are referred to as *B' Mop2/mop2-1.* Wild type *B'* and *B-I* are referred to as *B'* and
180 *B-I.*
181
182 ***B'* expression levels are increased in *mop1* and *mop3*, but not *mop*2 mutants**
183 To monitor the *b1* gene expression levels in the *mop* mutants in our greenhouse conditions,
184 we performed RNA blot analysis using seedling and husk tissue from the mutants as well as
185 *B'* and *B-I* wild type individuals as comparison.
186 In seedling tissue of *B' mop1-1, B' Mop2/mop2-1, B' mop2-1*, *B' mop3-1* and *B-I* no
187 expression of *b1* could be detected (triplicate samples; data not shown). As reported
188 previously, in wild-type husk tissue, in which the *b1* gene is transcriptionally activated, the *B'*

189 allele was lowly expressed, while *B-I* transcript levels were increased ~20-fold compared to
190 the *B'* levels (Figure 1) (Louwers et al., 2009a). In husk tissue from *B' mop1-1* and *B' mop3-*
191 *1*, the *b1* expression levels were ~3 fold and ~5-fold increased relative to that in *B'* plants,
192 respectively (Figure 1). The latter upregulation is in line with an 8-fold increase of *B'*
193 transcription in husk tissue observed in an *rmr6-1* mutant (Erhard et al., 2009; Hollick et al.,
194 2005). Both *B' mop1-1* and *B' mop3-1* adult plants display as intensely dark purple tissues as
195 *B-I* wildtype plants, indicating that the *b1* RNA expression levels in all three genotypes are
196 above a threshold needed to activate the maize pigmentation pathway. In *B' Mop2/mop2-1*
197 husk tissue, expression of *B'* remained low, while the expression in *B' mop2-1* and *B' mop2-2*
198 was slightly higher, in line with (slightly) higher pigment levels (Figure 1 and Supplemental
199 Figure S1**)**. In conclusion, although all three mutations prevent paramutation between *B'* and
200 *B-I*, the RNA blot data shows they have different effects on the *B'* expression level.
201
202 **Regulatory sequences at the *b1* locus are activated in *B' mop1-1* and *B' mop3-1***
203 To test whether changes in *b1* transcript level in *B' mop1-1*, *B' mop2* and *B' mop3-1* plants
204 are mediated by the activation of the previously identified distant regulatory sequences at the
205 *b1* locus (Belele et al., 2013; Louwers et al., 2009a; Stam et al., 2002a), we performed
206 chromatin immunoprecipitation (ChIP) with an anti-histone H3K9K14 acetylation (H3ac)
207 antibody on chromatin isolated from husk, tissue in which the *b1* gene is transcriptionally
208 activated. The precipitate was analyzed by quantitative PCR (qPCR) and normalized to *actin1*
209 values (Haring et al., 2007). The targeted genomic regions are shown in Figure 2A, and
210 Supplemental Figure S2; the primers used are listed in Supplemental Table S1. Compared to
211 the levels in *B'* wild-type, elevated levels of H3ac were clearly observed in husk tissue of *B'*
212 *mop1-1* and *B' mop3-1* at the *b1* locus (Figure 2B; Supplemental Figure S3 and Supplemental
213 Table S2), whereby the H3ac levels at the hepta-repeat where generally higher in *B' mop3-1*
214 than *B' mop1-1* tissue. This is in line with the higher *B'* expression levels in *mop3-1*
215 compared to *mop1-1*. The H3ac levels in both genotypes were, however, generally still
216 significantly lower than in the highly transcribed *B-I* genotype, indicating that the enhancer
217 sequences at the *b1* hepta-repeat are intermediately activated in *mop1-1* and *mop3-1* plants. In
218 line with low *B'* transcript levels, in heterozygous and homozygous *mop2-1* mutants, *B'*
219 showed only very low H3ac levels at the hepta-repeat and other regions at the *b1* locus,
220 similar as seen for *B'* in a wild-type background (Figure 2B; Supplemental Figure S3 and
221 Supplemental Table S2). In conclusion, the higher *b1* transcript levels in *B' mop1-1* and *B'*

222 *mop3-1* husk tissue are associated with higher histone acetylation levels at the hepta-repeat,
223 indicating activation of the distant regulatory sequences
224 at the *b1* locus.

225 **Activated *b1* regulatory sequences are associated with a multi-loop structure**

226 The low expression level of the *B'* epiallele in husk tissue has been associated with the
227 formation of a single loop between the *b1* TSS and hepta-repeat 100 kb upstream, whereas
228 transcriptional activation of the high expressed *B-I* epiallele has been associated with the
229 formation of a multi-loop structure between the TSS and regulatory regions ~15, ~47, ~100
230 and ~107 kb upstream (Louwers et al., 2009a). To examine if the activation of the regulatory
231 sequences at the *b1* locus in the *mop* mutants is associated with the formation of a multi-loop
232 structure, chromosome conformation capture (3C) was applied, using husk tissue from *B-I*, *B'*
233 (Louwers et al., 2009a) and *B' mop1-1*, *B' Mop2/mop2-1* and *B' mop3-1* plants, and *Bgl*II as
234 restriction enzyme. 3C allows the identification of physical interactions between selected
235 genomic regions. The TSS (fragment 1), hepta-repeat (fragment X) and a fragment ~47 kb
236 upstream (fragment VII) were used as a viewpoint (bait) (Figure 3, Supplemental Figure S2).
237 The *S-adenosyl methionine decarboxylase* (*Sam*) locus was used as an unrelated, internal
238 control for data normalization (Louwers et al., 2009a).

239 Our data show that in *mop1-1* and *mop3-1* husk tissue, the *B'* epiallele shows a *B-I*-
240 like multi-loop conformation, whereas in *Mop2/mop2-1* tissue *B'* shows a *B'*-like single-loop
241 conformation (Figure 3A-C). When using fragment I (*b1* TSS) as viewpoint, in all samples
242 the hepta-repeat (fragment X) showed high interaction frequencies (Figure 3A), whereby the
243 *B'* epiallele showed the lowest interaction frequencies in a wild-type and *Mop2/mop2-1*
244 background, and the highest in a *B' mop3-1* and *B-I* background. In addition, fragment I also
245 interacted with fragments XII (-107 kb), VII (-47 kb), and VI (-40 kb) and IV (-15 kb),
246 whereby high interaction frequencies with fragments VII, VI and IV where only observed in
247 *B' mop1-1*, *B' mop3-1* and *B-I* tissue, consistent with a multi-loop structure. When using
248 fragment X and VII as viewpoints (Figure 3, B and C), the high interaction frequencies
249 between the TSS, hepta-repeat and regions ~47, and ~15 kb upstream were confirmed for *B'*
250 *mop1-1* and *B' mop3-1*. The interactions involving the region ~107 kb upstream were
251 confirmed for all genotypes, with *B'* in a wild type and *Mop2/mop2-1* background showing
252 the lowest interaction frequencies.

253 In summary, our 3C data show that the transcriptional enhancement of *B'* expression
254 in the *mop1-1* and *mop3-1* mutant background is associated with the formation of a *B-I*-like

255 multi-loop structure, whereas the low *B'* expression level in the *Mop2/mop2-1* background is
256 associated with a *B'*-like single-loop structure as observed.
257
258 ***B'* hepta-repeat DNA methylation level is retained in all *mop* mutants**
259 At RdDM-target loci, the *mop1, mop2* and *mop3* genes have been indicated to play a major
260 role in maintaining CHH methylation (mCHH), and a minor role in maintaining CG and CHG
261 methylation (mCG, mCHG) (Gent et al., 2014; Li et al., 2015, 2014). In these studies, a
262 decrease in mCG and mCHG seemed most prominent in a *mop3* and least prominent in a
263 *mop2* mutant. Previous experiments showed that the silenced *B'* allele is DNA
264 hypermethylated at the hepta-repeat junction regions compared to *B-I* (Haring et al., 2010).
265 To examine if transcriptional activation of *B'* in *mop* mutants is associated with a decrease in
266 DNA methylation, DNA blotting and bisulfite sequencing experiments were performed.
267 DNA blot analyses were performed as described in Haring *et al.* (2010), using
268 genomic DNA from leaf and husk tissue, isolated from 4 to 27 individuals per genotype at
269 different stages of development. DNA was isolated and digested with *Eco*RI or *Bam*HI, which
270 released a discrete fragment containing the entire hepta-repeat, and eight different methylation
271 sensitive restriction enzymes (Figure 4), size fractionated, blotted and hybridized with a
272 repeat probe (for representative examples, and the sequence and sites examined see
273 Supplemental Figure S2, S4 and S5). To check for complete digestion, probes recognizing
274 unmethylated sequence regions within the *b1* locus were used. To approximate the DNA
275 methylation levels, relative band intensities of all detected restriction fragments were
276 computationally compared to all theoretical possible combinations of fragment intensities.
277 Compared to *B'* tissue, in *B' mop1-1* and *B' mop3-1* tissue we observed only a slight
278 decrease in DNA methylation level at the *B'* repeat junction regions, with the most decrease
279 observed in *B' mop3-1* tissues (Figure 4, Supplemental Figure S4 and S6). The decrease
280 occurred in several, but not all plants, and was observed at specific restriction sites, in a
281 stochastic manner; a decrease at a particular site was not necessarily associated with a
282 decrease at another site in the same sample. In *B' Mop2/mop2-1, mop2-1* as well as *mop2-2*
283 samples, no decrease in DNA methylation was observed at the hepta-repeat (Figure 4,
284 Supplemental Figure S4 and S6).
285 In addition to the slight decrease in DNA methylation, in most *B' mop1-1* and all *B'*
286 *mop2* samples we detected hypermethylation at the repeat junctions (Figure 4 and
287 Supplemental Figure S4 and S6; *Hha*I and *Hae*II). In the *mop3-1* mutant, however, a

288 stochastic decrease in DNA methylation was observed at the site hypermethylated in the
289 *mop1-1* and *mop2* mutants.

290 We expected that during the development of *B' mop1-1* plants, as previously
291 hypothesized (Ohtsu et al., 2007), a progressive decrease in DNA methylation levels would
292 be observed due to cell division. To test this hypothesis, DNA blot analysis was performed on
293 DNA from six to eight leaves collected during the development of six homozygous *B' mop1-*
294 *1* plants (Supplemental Figure S7). In most plants monitored (5 of 6), we did detect a slight
295 decrease in DNA methylation, but in general, the maximum decrease in DNA methylation
296 was already observed in the second leaf stage, suggesting that this reduction in DNA
297 methylation may already have occurred in very early developmental stages such as embryos,
298 in which *Mop1* appears higher expressed compared to seedlings and leaves (Sekhon et al.,
299 2011; Woodhouse et al., 2006b).

300 DNA methylation at the *B'* repeat junction regions in *mop1-1*, *Mop2/mop2-1* and
301 *mop3-1*, and *B'* and *B-I* wild type was also monitored by targeted bisulfite sequencing, which
302 provides single base-pair resolution data on cytosine methylation. DNA was obtained from
303 leaf 4 tissue of V4 stage plants, and *Fie2* was used as a control for complete conversion
304 (Gutiérrez-Marcos et al., 2006). As observed with DNA blot analysis, the *B'* repeat junction
305 region was hypermethylated compared to that of *B-I*, both in wild-type and *mop* mutant leaf
306 tissue (Figure 4B, Supplemental Figure S8). Bisulfite sequencing confirmed the lack of
307 significant DNA demethylation in the *mop* mutants. In fact, there was no detectable decrease
308 in DNA methylation. This difference from the DNA blot analysis method could be due to the
309 limited number of samples that can be easily examined by targeted bisulfite sequencing. Also
310 note that bisulfite sequencing represents individual molecules in individual cells while DNA
311 blot analysis represents large population of cells. In addition, there may be variation between
312 the seven repeats, and DNA blot analyses provide the overall picture. Intriguingly, in contrast
313 to the expectations (Li et al., 2014), the vast majority of DNA methylation observed at the *B'*
314 allele was in the CG and CHG context, and the low level in the CHH context (3%) was
315 similar in *B-I* and *B' mop* samples (Figure 4B and C, Supplemental Figure S8). These
316 findings are in contrast to reported observations that the RdDM pathway, in which the MOP
317 proteins play a role, mediates *de novo* DNA methylation in all sequence contexts, including
318 CHH (Gent et al., 2014; Li et al., 2015, 2014; Matzke and Mosher, 2014).

319 Together, our data indicate that i) activation of the enhancer function of the hepta-
320 repeat occurs in the presence of high DNA methylation levels, ii) the MOP proteins plays a

321 minor role in maintaining DNA methylation at the *b1* hepta-repeat, and iii) the *B'* repeat
322 junction regions show very low mCHH levels.
323
324 **Genome-wide variation in mCHH levels exists at RdDM loci**
325 Our finding that the *B′* repeat junction region, which is likely to be an RdDM locus, has little
326 mCHH, prompted us to explore whether similar loci, with MOP1-dependent 24-nt siRNAs,
327 but little mCHH, are present elsewhere in the genome. To do this, we used published small
328 RNA and DNA methylation datasets from wild-type and *mop1-1* mutant developing ear (Gent
329 et al., 2014). First, we compared the abundance of perfect-matching, uniquely-mapping 24-nt
330 siRNAs across the maize B73 genome to identify loci with abundant siRNAs in wild-type and
331 at least ten-fold reduced coverage in the *mop1-1* mutant. We then categorized all identified
332 loci based on mCHH levels in developing ear, whereby loci with mCHH values of less
333 than 0.02 (mC/total C) were categorized as low mCHH *mop1* loci, and greater than or equal
334 to 0.02 were categorized as high mCHH *mop1* loci. For increased stringency, we used 50-bp
335 non-overlapping intervals across the genome, and only included loci where at least two
336 adjacent loci were both low or both high mCHH. All adjacent 50-bp loci fitting the same
337 category were then merged, producing 69 low mCHH *mop1* loci and 3107 high mCHH *mop1*
338 loci, all of which were at least 100-bp in length (Supplemental Figure S9). Note that these
339 numbers are certainly smaller than the actual numbers of such loci in the genome. For this
340 analysis, our aim was to determine whether the *b1* enhancer is an anomaly, not to rigorously
341 identify and categorize all *mop1* loci in the genome. Excluding multi-mapping siRNAs is the
342 largest limiting factor of this analysis, but was necessary for robust interpretation of the data.
343 Based on these numbers, approximately 2% of *mop1* loci have low mCHH levels, like
344 observed for the *B′* repeat junction region. While both the low and high mCHH *mop1* loci had
345 high abundance of 24-nt siRNAs, the siRNAs at high mCHH loci were on average about two-
346 fold more abundant than at low mCHH loci. Both sets were dominated by 24nt siRNAs,
347 though other lengths were also present and were also similarly more abundant at high mCHH
348 loci (Supplemental Figure S9).
349 In whole-genome studies like this, selecting for the tails of a distribution (in this case
350 low mCHH) will always yield some number of false positives. To evaluate whether the loci
351 we identified have reproducibly low mCHH, we used data from a different tissue (developing
352 second leaf), produced using a different method (enzymatic conversion rather than bisulfite
353 conversion) (Hufford et al., 2021). In spite of a general reduction in mCHH in leaf compared
354 to ear, the general patterns were highly reproducible, not just for mCHH, but also mCG and

355 mCHG (**Figure 5**). In particular, the mean mCHH in leaf was 0.02 in low mCHH loci, but
356 0.10 in high mCHH loci, and both mCG and mCHG showed high, heterochromatin-like levels
357 in both sets of loci (Gent et al., 2014). These data also indicate that the majority of low
358 mCHH loci with MOP1-dependent siRNAs in ear also have low mCHH in leaf.
359

360 **Transcriptional activation is not associated with a decrease in nucleosome occupancy at**
361 **the *B'* repeats**

362 Nucleosome occupancy plays an important role in gene regulation (Jiang and Pugh, 2009;
363 Struhl and Segal, 2013), with nucleosome depletion at regulatory regions being associated
364 with gene expression. To test whether the increased *B'* expression level in *mop1-1* and *mop3-*
365 *1* plants (Figure 1) is associated with decreased nucleosome occupancy, ChIP-qPCR
366 experiments were performed using an anti-histone H3 antibody (H3core) that recognizes
367 canonical H3 and H3 variants. As observed before, the hepta-repeats display a low and high
368 nucleosome occupancy in *B-I* and *B'* husk, respectively (Figure 6, Supplemental Figure S10)
369 (Haring et al., 2010). This is consistent with the hepta-repeat acting as a transcriptional
370 enhancer in *B-I*, but not *B'* plants. In husk tissue of *B' mop1-1* plants, however, compared to
371 *B*' wildtype plants no significant differences in nucleosome occupancy level were observed at
372 the hepta-repeat; they were significantly different from those in *B-I* plants, but not *B'* plants
373 (Figure 6, Supplemental Figure S10, Supplemental Table S2). This indicates that in *B' mop1-*
374 *1*, the increased *B'* RNA level is not facilitated by nucleosome displacement. The histone H3
375 levels at the hepta-repeat in *B' mop3-1* plants were not significant different from both *B*' and
376 *B-I* plants, indicating they were at an intermediate level and the elevated *B'* RNA levels in *B'*
377 *mop3-1* plants could be slightly facilitated by nucleosome displacement. *Mop2/mop2-1* plants
378 showed similar results at the *B'* hepta-repeat as *mop1-1* plants, while *mop2-1* homozygous
379 plants showed H3core levels that were significantly different from both *B'* and *B-I* wildtype.
380 They were higher than in *B'*.
381

382 **Transcriptional activation is associated with reduced H3K9me2 and H3K27me2 levels**

383 The silencing of transposons and other repeats is associated with DNA methylation,
384 H3K9me2 and H3K27me2 (Bernatavichute et al., 2008; Gent et al., 2014; Liu et al., 2021;
385 Roudier et al., 2011; West et al., 2014). In maize, H3K9me2 and H3K27me2 are both
386 enriched in heterochromatin, and they are enriched at low and moderately expressed genes,
387 respectively (relative to highly expressed genes) (Gent et al., 2014). Our previous study
388 indicated that the *B'* gene body is marked by H3K27me2 in both seedling and husk tissue,

389 while the *B'* hepta-repeat carries H3K9me2 and H3K27me2 only in husk (Haring et al.,
390 2010). To examine if activation of the *B'* epiallele in *mop* mutant plants is associated with
391 reduced H3K9me2 and H3K27me2 levels, ChIP-qPCR experiments were performed on
392 seedling and husk tissue, using monoclonal antibodies with a much better signal-to-noise ratio
393 than the antibodies used in our previous study (Figure 7, see Methods) (Haring et al., 2010).
394 The *B'* and *B-I* epialleles are transcriptionally activated in husk, but not in seedling tissue. A
395 high-copy *Copia* sequence was used to normalize the data (Haring et al., 2010, 2007).
396 Unlike our previous results, H3K9me2 was significantly enriched at the hepta-repeat
397 in *B'* seedling as well as husk tissue, suggesting that the *B'* hepta-repeat is marked by
398 H3K9me2 in a tissue-independent manner (Figure 7A, B, Supplemental Figure S11A, B). The
399 *b1* gene itself in the *B'* epiallelic state did not show significant H3K9me2 levels, nor in the *B-*
400 *I* epiallele. In line with H2K27me2 being associated with repressed sequences, H3K27me2
401 levels were significant enriched at the hepta-repeat, gene body and other sequences in *B'* and
402 *B-I* seedlings, and *B'* husk tissue, tissue in which the *b1* gene is not activated (Figure 7C, D,
403 Supplemental Figure S11C, D, Supplementary Table S2). In *B-I* husk tissue, where *b1*
404 transcript levels are high (Figure 1), only background levels of H3K27me2 were detected
405 across the *b1* locus.
406 In seedling tissue, in which the *b1* gene is transcriptionally inactive, the H3K9me2
407 levels were significantly lower at the *B'* hepta-repeat in *mop3-1* plants than in wild type *B'*
408 plants (Figure 7A, C, Supplemental Table S2). The same is true for the H3K27me2 levels for
409 both *mop1-1* and *mop3-1* seedlings. In husk tissue, both the H3K9me2 and H3K27me2 levels
410 were significantly lower in *mop1-1* and *mop3-1* plants compared to wild type *B'* plants
411 (Figure 7B, D and Supplemental Figure S11B, D, Supplementary Table S2). The significant
412 decrease in H3K9me2 (*mop3-1*) and H3K27me2 (*mop1-1* and *mop3-1*) levels at the hepta-
413 repeat is already observed in seedling tissue and therefore independent of transcriptional
414 activation of the *b1* gene, suggesting this decrease is a true effect of these *mop* mutations. At
415 the gene body (UTR, Ex3), only the H3K27me2 levels in *B' mop3-1* husk tissue were
416 significantly different from those in wild-type *B'* plants, in line with the relatively high
417 expression level in *B' mop3-1* plants. The increased *b1* expression levels in *B' mop1-1* husk
418 tissue occurs without a significant decrease of H3K27me2 levels at the gene body.
419 In *Mop2/mop2-1*, *mop2-1* husk tissue, similar levels of H3K9me2 and H3K27me2
420 were observed at the *B'* hepta-repeat as in wild type *B'* tissue (Figure 7B, D and Supplemental
421 Figure S11B, D, Supplementary Table S2). H3K27me2 levels at the *b1* coding region were
422 also not significantly different. These observations were confirmed using the independent

423 *mop2-2* mutant, showing that the results are not specific for a dominant mutation like *mop2-1;*
424 repressive chromatin marks at the *B'* epiallele are also retained in the *mop2-2* mutant.
425 In conclusion, in *mop1-1* and *mop3-1* mutants the repressive H3K9me2 and/or
426 H3K27me2 marks are reduced at the *B'* hepta-repeat. For H3K9me2, this reduction is tissue-
427 independent for *mop3-1*, while for H3K27me2 this is true for both mutants. We propose that
428 these lower levels allow transcriptional activation of the *B'* epiallele in husk tissue. The
429 retention of these marks in *mop2* mutants correlates with the lack of a significant increase in
430 *B'* transcript levels in these mutants.

431 # Discussion

432 In this study we show that the RNA-dependent RNA polymerase (RdRP, MOP1) and the
433 largest subunit of RNA polymerase IV (NRPD1, MOP3), proteins in the RNA-directed DNA
434 methylation (RdDM) pathway, are involved in maintaining high levels of the repressive
435 histone marks H3K9me2 and H3K27me2 at the *b1* regulatory hepta-repeat, but not in
436 maintaining high DNA methylation levels. In the *mop1* and *mop3* mutants strong and
437 reproducible reductions in the levels of the repressive H3K9me2 and H3K27me2 histone
438 marks are detected at the regulatory hepta-repeat enhancer, but only weak and stochastic
439 reductions in DNA methylation. We also show that *mop1* and *mop3* mutants, which prevent
440 paramutation at multiple maize loci including *b1*, allow partial activation of the regulatory
441 hepta-repeat enhancer at the *B'* epiallele in the presence of high DNA methylation and
442 nucleosome occupancy levels.
443
444 *Role of MOP proteins in maintenance of DNA methylation*
445 Mutations in *Mop1* (RdRP), *Mop2* (NRP(D/E)2a), and *Mop3/Rmr6* (NRPD1) prevent
446 paramutation and significantly reduce overall 24-nt siRNAs levels (Arteaga-Vazquez et al.,
447 2010; Erhard et al., 2009; Nobuta et al., 2008; Sidorenko et al., 2009; Stonaker et al., 2009).
448 The *mop1-1* and *mop2-1* mutants have in addition been shown to significantly reduce the
449 levels of hepta-repeat-derived 24-nt siRNAs (Arteaga-Vazquez et al., 2010; Sidorenko et al.,
450 2009). We, however, did not observe significant reductions in mCG and mCHG at the repeat
451 junction region in any of the mutants examined. Earlier studies in maize did report reductions
452 in DNA methylation at so-called mCHH islands, whereby decreases were more severe in
453 *mop3-1* than *mop1-1* plants and more in mCHG than in mCG (Gent et al., 2014; Li et al.,
454 2014). In addition, studies in Arabidopsis, showed decreased mCHG and mCG levels in *rdr2*,
455 and *nrpd1* mutants (Tang et al., 2016; Zemach et al., 2013). We only observed stochastic

456 decreases in DNA methylation with our DNA blot analyses in *mop1-1* and *mop3-1* mutants,
457 and to a larger extent in *mop3-1* than *mop1-1* plants. Not all plants, however, showed such
458 decrease at the restriction sites monitored, therefore, the activation of the hepta-repeat
459 enhancer in these mutants is only weakly associated with non-reproducible decreases in DNA
460 methylation.
461
462 *Role for RdDM components in maintenance of repressive histone modifications.*
463 The activation of the enhancer at the *B′* hepta-repeat in the *mop1-1* and *mop3-1* mutants is
464 associated with significant reductions in the repressive H3K9me2 and/or H3K27me2 marks.
465 Given the well-established roles for siRNAs in directing DNA methylation, the reductions in
466 these histone modifications would normally be explained as a downstream consequence of
467 loss of DNA methylation. In principle, the MOP siRNA machinery could also directly target
468 H3K9me2 or H3K27me2 through unidentified protein-protein interactions between argonaute
469 proteins and histone methyltransferases. Such a scenario is supported by the existence of
470 RNA-directed histone modification without RNA-directed DNA methylation in diverse fungi
471 and animals, including *Drosophila melanogaster*, *Caenorhabditis elegans* and
472 *Schizosaccharomyces pombe* (Castel and Martienssen, 2013; Gu et al., 2012; Pal-Bhadra et
473 al., 2004; Verdel et al., 2004). In addition, a few studies have implicated siRNAs in directing
474 H3K9me2 in Arabidopsis (Jackel et al., 2016; Parent et al., 2021), although effects on
475 H3K9me2 and DNA methylation could not be unequivocally disentangled.
476 Interestingly, it has been shown that tandem repeats are efficiently and stably silenced
477 by H3K9 methylation through RNA-mediated mechanisms (Grewal, 2023). Small RNAs
478 derived from only one or a limited number of repeats can target all the repeats at a given locus
479 and mediate a high density of H3K9 methylation, which in turn recruits histone deacetylases
480 (HDACs) that stabilize heterochromatic regions (Grewal, 2023; Zofall et al., 2022). Similarly,
481 small RNAs may be required to target high H3K9me2 levels at the hepta-repeat, which in turn
482 recruits HDACs stabilizing the silencing.
483 Resolving the hierarchy of histone methylation and DNA methylation is complicated
484 by indirect effects of developmental gene regulation. In husk, where the hepta-repeat serves
485 as a weak enhancer for the *b1* gene in the mutants, we expect that some of the reduction in
486 histone methylation is due to the presence of transcription factors and associated chromatin
487 modifiers. In seedling tissue, however, in which *b1* is transcriptionally repressed, the
488 reduction should be independent of transcriptional activation of *b1*. Thus, the stronger

489 reduction of H3K27me2 over H3K9me2 in *B' mop1-1* seedling could suggest a more direct
490 effect of the MOP siRNA pathway on H3K27me2.

491 A clear link between H3K27me2 and RdDM in plants has not been shown before.
492 H3K27me2 is, as H3K27me3, intimately associated with transcriptional silencing through
493 Polycomb group (PcG) proteins (Conway et al., 2015). While H3K27me3 is mainly
494 associated with repressed genes, H3K27me2 is localized more ubiquitously throughout the
495 genome. Data from animals indicate that, unlike H3K27me3, H3K27me2 is not associated
496 with stable binding of Polycomb Repressive Complex 2 (PRC2); it is indicated to act as a
497 protective layer against unspecific transcriptional activation (Ferrari et al., 2014; Lee et al.,
498 2015). This includes preventing the activation of enhancer sequences in inappropriate cell
499 types. In agreement with these findings, in Arabidopsis and maize, H3K27me2 is enriched at
500 silenced promoters, genes and repeats (Gent et al., 2014; Locatelli et al., 2009; Mathieu et al.,
501 2005; Park et al., 2012; Roudier et al., 2011), and in wheat at euchromatic transposons at
502 distal chromosome ends (Liu et al., 2021). In Arabidopsis, H3K27me2 enrichment seems
503 independent of the presence of H3K9me2 or DNA methylation (Mathieu et al., 2005), and in
504 wheat mutually exclusive with H3K9me2 (Liu et al., 2021), suggesting that H3K27me2 and
505 RdDM are independent of each other. In line with this idea, in maize, high H3K27me2 levels
506 are observed at both RdDM and non-RdDM loci (Gent et al., 2014). In maize
507 heterochromatin, however, H3K27me2 largely overlaps with H3K9me2 and DNA
508 methylation, except that H3K27me2 is found at more loci (Gent et al., 2014). Links between
509 small-RNA mediated transcriptional silencing and H3K27 methylation have been observed in
510 protozoa. In *Tetrahymena thermophila*, small-RNA dependent recruitment of H3K27me3 to
511 developmentally transcriptionally silenced loci has been observed (Liu et al., 2007). A strong
512 relation between H3K27me2 enrichment and small RNA-mediated transcriptional silencing
513 has been observed in the protozoan *Entamoeba histolytica* (Foda and Singh, 2015). Here we
514 show that in *B' mop1-1* and *mop3-1* plants, the H3K27me2 levels at the hepta-repeat are
515 significantly lower than in *B'* wild type plants, suggesting that in maize MOP factors can
516 mediate RNA-directed histone methylation.

517 Our observation of *mop* mutants resulting in reduced H3K27me2 and H3K9me2 levels
518 does not resolve the relationship and potential hierarchy between these two histone
519 modifications. It is also possible that the MOP siRNA pathway recruits more than one histone
520 methyltransferase. In this scenario, both H3K27 and H3K9 could be direct targets, whereby
521 the respective histone methyltransferases may be recruited at different levels in different
522 tissues. Regardless of which histone modifier could be part of the MOP siRNA pathway at the

523 *b1* hepta-repeat, it is likely not an anomaly. Our finding that 2% of *mop1* siRNA loci have
524 low levels of mCHH is consistent with a common function of 24-nt siRNAs in something
525 other than directing DNA methylation.
526
527 *Reinforcing cycle between mCHG and H3K9me2*
528 How could a large role for siRNAs in directing histone modifications go unnoticed? For one
529 reason, it is difficult to separate DNA methylation from histone modifications, especially
530 given the massive pleiotropic effects of mutants. At the *b1* hepta-repeat, however, we
531 observed a tissue-independent decrease in H3K9me2 in *mop3-1*, while mCHG remains high.
532 mCHG is normally tightly linked to H3K9me2 because chromomethylases (CMTs) bind
533 H3K9me2 containing nucleosomes and methylate cytosines in the CHG context (Bartee et al.,
534 2001; Du et al., 2014, 2012; Lindroth et al., 2001; Stroud et al., 2014, 2013). In addition,
535 H3K9 histone methyltransferases bind to methylated cytosines to methylate H3K9 (Du et al.,
536 2014; Johnson et al., 2007). In maize, the CMTs ZMET2 and ZMET5 are required for mCHG
537 (Fu et al., 2018; Gent et al., 2014; Li et al., 2014; Papa et al., 2001); ZMET2 also binds
538 H3K9me2 (Du et al 2012). At the *B'* hepta-repeat, CHG methylation is, however, not
539 decreased in *mop1-1* and *mop3-1* mutants, while H3K9me2 is significantly decreased,
540 suggesting that CHG methylation is not sufficient to recruit H3K9 methyltransferases to
541 maintain high H3K9me2 levels at the *B'* hepta-repeat. This supports the idea that the MOP1
542 RdRP and especially MOP3 NRPD1 play a role in recruiting H3K9 methyltransferases. It is
543 unclear, however, how the high mCHG levels are maintained. Possibly, the reduced levels of
544 H3K9me2 are still sufficient for ZMET2/5 to maintain high mCHG levels.
545
546 *Gene activation in presence of repressive marks*
547 Previously, we postulated that low DNA methylation levels and lack of H3K9me2 and
548 H3K27me2 at the *B-I* hepta-repeat would allow the binding of transcription factors driving
549 activation of the hepta-repeat enhancer (Haring et al., 2010; Louwers et al., 2009a). We
550 showed that activation of the *B-I* hepta-repeat enhancer was associated with histone
551 acetylation and chromosomal interactions between the hepta-repeat, TSS and additional
552 regulatory sequences at the *b1* locus, ultimately resulting in tissue-specific transcriptional
553 enhancement of *b1*. The repressive marks at the *B'* hepta-repeat, DNA methylation,
554 H3K9me2, and H3K27me2 were hypothesized to hamper enhancer activation and block the
555 formation of a multi-loop structure, resulting in low *b1* expression. Accordingly, the presence
556 of these repressive epigenetic marks are also negatively correlated with enhancer activity in

557 other systems (Ferrari et al., 2014; Plank and Dean, 2014; Schmitz et al., 2022; Sekhon et al.,
558 2012; Xie et al., 2013). Here we show the remarkable finding that, in *mop1-1* and *mop3-1*
559 mutant plants, the regulatory sequences at the *b1* locus can be activated in the presence of
560 high levels of DNA methylation and nucleosomes. This activation is illustrated by increased
561 *b1* RNA and H3ac levels, and the formation of a multi-loop structure at the *B'* epiallele (Figs.
562 1-3). The restoration of the *b1* expression is, however, only to about 15% (*mop1-1*) or 23%
563 (*mop3-1*) of the *B-I* level (Figure 1). Accordingly, the H3ac levels are (slightly) lower than
564 observed for *B-I*. We hypothesize that in *B' mop1-1* or *mop3-1* husk tissue, a reduction in
565 H3K9me2 and H3K27me2 levels at each hepta-repeat is sufficient to allow transcription
566 factors and other protein factors involved in enhancer function to bind the hepta-repeat, albeit
567 with a relatively low affinity. This then results in an intermediately active enhancer that can
568 physically interact with the additional regulatory sequences, ~107, ~47 and ~15 kb upstream
569 of the TSS; together they mediate the formation of an active transcription complex at the *b1*
570 promoter, upregulating *b1* transcription. Alternatively, there could be near 100% reduction of
571 H3K9me2 and H3K27me2 at a limited number of *b1* alleles, activating *b1* expression in only
572 a fraction of cells. In either case, the high DNA methylation levels at the hepta-repeat
573 enhancer allow the binding of proteins involved in enhancer activation to some extent.
574 Unlike in the *mop1-1* and *mop3-1* mutants, in both the dominant and recessive *mop2*
575 mutants there is no significant decrease in H3K9me2 and H3K27me2 at the hepta-repeat
576 enhancer, and the DNA methylation levels are, if anything, even slightly increased. Retention
577 of these repressive marks in *mop2* mutants correlates with a lack of enhancer activation,
578 which is associated with the formation of a single loop structure and no significantly
579 increased *B'* transcript levels in these mutants. *Mop2/Rmr7* codes for NRP(D/E)2a, the
580 second largest subunit of Pol IV and Pol V (Sidorenko et al., 2009; Stonaker et al., 2009).
581 NRP(D/E)2a has two paralogs, NRP(D/E)2b and NRPE2c. NRP(D/E)2b is also part of Pol IV
582 and V while NRPE2c is only part of Pol V (Haag et al., 2014; Sidorenko et al., 2009).
583 Nevertheless, neither of these paralogs is able to substitute for NRP(D/E)2a with respect to
584 paramutation in terms of the establishment of DNA and histone methylation at the *b1* hepta-
585 repeat. However, one of the paralogs may substitute for NRP(D/E)2a to maintain these marks.
586 Arabidopsis contains one functional homologue of NRP(D/E)2a, (NRP(D/E)2; (Herr et al.,
587 2005; Kanno et al., 2005; Onodera et al., 2005; Pontier et al., 2005)). DNA blot analysis on
588 Arabidopsis mutants of NRP(D/E)2 indicated a slight decrease in DNA methylation at 5S
589 genes. So far, no effects on histone modifications are reported. In conclusion, our results

590 indicate that repression of the *B'* epiallele can be maintained independent of MOP2 but does
591 require MOP1 and MOP3.
592
593 *Effect on chromatin structure by mop mutants*
594 The different *mop* mutants all hamper paramutation and block RdDM, but affect the
595 chromatin structure differently. In the *mop1-1* and *mop3-1* mutants, repression at the *B'*
596 hepta-repeat enhancer is released to different extents, but not in *mop2* mutants. We know little
597 about the effect of these mutants on the binding of the RdDM components that are still
598 functional. We expect, like observed for Arabidopsis, the MOP1 RdRP to stably bind the
599 largest subunit of Pol IV (NRPD1/Mop3/Rmr6) (Law et al., 2011; Mishra et al., 2021). The
600 effect of a lack of a functional MOP1 on the binding of the remaining RdDM components to
601 chromatin in a *mop1-1* mutant is unknown.
602 We hypothesize that in a *mop3* mutant, Pol V, but not Pol IV, is still functional,
603 resulting in transcription of the *B'* hepta-repeat by Pol V in the absence of RdDM. This
604 transcription may lead to the observed decrease of H3K9me2 and H3K27me2 at the *B'* hepta-
605 repeat, allowing enhancer activation. In line with this hypothesis, in Arabidopsis the
606 production of Pol V transcripts is independent of mutations affecting components in siRNA
607 biogenesis, and *de novo* and maintenance DNA methylation (DICER1-4, RDR2, DRM2,
608 MET1 and DDM1) (Wierzbicki et al., 2008).
609 As discussed above, we cannot exclude that in *mop2* mutants, NRP(D/E)2a is replaced
610 by NRP(D/E)2b or 2c, which may still be able to repress the *B'* hepta-repeat. Alternatively,
611 both Pol IV and Pol V become non-functional and in absence of their transcription activity,
612 the *B'* hepta-repeat stays repressed. In Arabidopsis, which has only one NRP(D/E), it has
613 been seen that in the absence of NRP(D/E)2, the largest subunit of Pol V is destabilized,
614 while NRPD1 is not (Pontier et al., 2005). If also true in maize, the Pol V protein complex
615 would no longer bind, while the Pol IV complex may be dysfunctional.
616 The dissimilar effect of *mop1*, *mop2* and *mop3* mutations on the repressed state of the
617 *B'* hepta-repeat is in line with findings for *pl1*. In 2-10% of wild-type plants, *Pl'*
618 spontaneously reverts to the *Pl-Rh* state (Hollick et al., 1995) and is therefore less stable than
619 the *B'* state, for which no reversion to *B-I* has been observed. In *rmr6-1* (*mop3*) mutants, *Pl'*
620 changes to *Pl-Rh* with an increased reversion rate of 36% (Hollick et al., 2005), and also in
621 *mop1-1* mutants a higher reversion rate to *Pl-Rh* was observed than in wild-type plants
622 (Dorweiler et al., 2000). In *rmr7* (*mop2*) mutants, however, *Pl'* does not revert to *Pl-Rh*,

623 indicating that the *Pl'* epiallele is more stably repressed in an *nrp(d/e)2a* mutant than in wild-
624 type plants (Stonaker et al., 2009).
625
626 *Epigenetic memory*
627 For *mop1-1* and *rmr6* (*mop3*) mutant plants, in which the production of siRNAs is severely
628 decreased (Arteaga-Vazquez et al., 2010; Erhard et al., 2009; Nobuta et al., 2008; Sidorenko
629 et al., 2009; Stonaker et al., 2009), it has been shown that the epigenetic memory of the
630 paramutagenic *B'* state is maintained (Dorweiler et al., 2000; Hollick et al., 2005). Upon
631 crossing out the *mop* mutations, *B'* can again paramutate *B-I* and is again lowly expressed,
632 indicating the RdDM pathway is not involved in maintaining the epigenetic memory. We
633 hypothesize that mCG and mCHG play a crucial role in maintaining the *B'* epigenetic state
634 through meiosis, as in all *mop* mutants, the *B'* hepta-repeat remains associated with high
635 mCG and mCHG levels. DNA methylation has been shown to play a central role in the stable
636 transgenerational inheritance of silent epigenetic states in plants (Fitz-James and Cavalli,
637 2022; Mathieu et al., 2007). In line with this, Calarco et al. (2012) showed that mCG and
638 mCHG are largely maintained in the germline. We, however, cannot entirely exclude a role
639 for H3K9me2 and H3K27me2, even when the *B'* hepta-repeat H3K27me2 levels are
640 significantly reduced tissue-independently in *mop1-1* and *mop3-1* mutants, and H3K9me2
641 levels in the *mop3-1* mutant. H3K9 methylation has been indicated to play a role in
642 transgenerational inheritance in *S. pombe*, *D. melanogaster* and *C. elegans* (Fitz-James and
643 Cavalli, 2022), and immunocytological data suggests that H3K9me2 may be retained during
644 meiosis (Underwood et al., 2018). Currently, there is no role reported for H3K27me2 in
645 transgenerational inheritance in plants.
646
647 *Concluding remarks*
648 This study showed that, in the presence of high DNA methylation, a reduction in the
649 repressive H3K9me2 and H3K27me2 marks at the regulatory *b1* hepta-repeat is sufficient to
650 allow partial activation of the hepta-repeat enhancer function. This indicates that the mere
651 presence of DNA methylation is not sufficient to entirely block enhancer function and that
652 high levels of H3K9me2 and H3K27me2 are involved in blocking enhancer function. We also
653 showed that high mCHG levels can be maintained in the presence of significantly reduced
654 H3K9me2 levels, suggesting the reduced H3K9me2 levels are still sufficient for ZMET2/5 to
655 maintain high mCHG levels. Intriguingly, we show that in maize, the RdRP and largest
656 subunit of RNA Pol IV involved in RdDM also play a role in the maintenance of H3K9me2

657 and H3K27me2. More experiments are necessary to show if this maintenance role is confined
658 to a limited number of sequences or occurs genome-wide. Our results also emphasize the
659 possibility of RNA-directed histone modification in plants, as occurs in diverse fungi and
660 animals. Future studies will be needed to examine the role of the MOP siRNA pathway in
661 H3K9me2 and H3K27me2, and if RNA-directed histone modifications play a role in
662 paramutation.
663
664

665 # Methods

666 **Genetic Stocks and Plant Materials**

667 The plants stocks used in this study (*B'/B' Mop1/Mop1* (K55), *B-I/B-I Mop1/Mop1* (W23),
668 *B'/B' Mop1/mop1-1* (K55/W23), *Mop2 B'/mop2-1 B'* (W23/K55), *Mop2 B'/mop2-2 B'*
669 (W23/K55), *B'/B' Mop3/mop3-1* (W23/K55) were obtained from V.L. Chandler (University
670 of Arizona, Tucson, AZ) and grown in greenhouse conditions. Homozygous *mop* mutants
671 were obtained by crossing *B'/B' mop1-1/Mop1* with *B'/B' mop1-1/mop1-1, Mop2 B'/mop2-1*
672 *B'* with *mop2-1 B'/mop2-1 B', Mop2 B'/mop2-2 B'* with *mop2-2 B'/mop2-2 B',* and *B'/B'*
673 *Mop3/mop3-1* with *B'/B' mop3-1/mop3-1*, respectively. Homozygous progeny were identified
674 using PCR genotyping (*mop1-1*) followed by sanger sequencing (*mop2*) and/or scoring
675 pigment levels (*mop1-1*, *mop3-1*) (Sidorenko et al., 2009; Sloan et al., 2014). Heterozygous
676 *B' Mop2/mop2-1* mutants for experiments were mainly obtained from a cross of *Mop2*
677 *B'/mop2-1 B'* with *mop2-1 B'/mop2-1 B'.* In addition, for a few RNA and DNA isolations also
678 samples from a cross between wild type *B'* and homozygous *mop2-1 B'* plants were used (data
679 in Supplemental Figure S1, S6; derivation is indicated in the figures). The seedling tissue
680 used for ChIP experiments comprised of 1-month-old seedlings with the roots and exposed
681 leaf blades removed. The husk tissues employed for RNA, ChIP and 3C consisted of all
682 leaves surrounding the maize ear, whereby the tough, outer leaves were discarded (Haring et
683 al., 2010; Louwers et al., 2009a). Husks were harvested at the time of silk emergence. For
684 DNA methylation analysis, mainly leaf blade tissue served as input material.
685

686 **RNA Analysis**

687 RNA blot analysis was performed as described previously (Louwers et al., 2009a; Haring et
688 al., 2010). RNA was isolated from husk tissue and 10 µg of RNA was size-fractionated by
689 formaldehyde gel electrophoresis, blotted and hybridized with probes against the *b1* or *Sam*

690 gene (Louwers et al., 2009a). RNA blots were hybridized with probes recognizing the coding
691 region of *b1* or *Sam*. Band intensities were quantified using a Storm 840 phosphorimager and
692 ImageQuant software (GE LifeSciences) and relative transcript levels of *b1* were calculated
693 by normalization to transcript levels of the *Sam* housekeeping gene.
694
695 **Chromatin Immunoprecipitation**
696 ChIP-qPCR experiments were performed on husk and seedling tissue as previously described
697 (Haring et al., 2010, 2007). Antibodies were used against H3K9ac/K14ac (Upstate #06-599),
698 H3K9me2 (Cell signaling #4658), H3K27me2 (Cell signaling #9728) and histone H3 (Abcam
699 #1791). For the no-antibody reactions, 20 µl Rabbit serum/ChIP sample (Sigma R9133) was
700 used. The specificity of the H3K9me2 and H3K27me2 antibodies was validated by slot blots
701 containing different dilutions of the target peptides (Egelhofer et al., 2011). All ChIP-qPCR
702 experiments were done using PLAT SYBR QPCR 500 (Invitrogen/Fisher, # 11733046) on an
703 Applied Biosystems™ 7500 Real-Time PCR System, repeated 2-4 times with chromatin
704 derived from different plants (see legends Figures 2,6 and 7, and Supplemental Figures S3,
705 S11, S11). Primers that were used for the qPCR analysis are listed in Supplemental Table S1.
706 *Actin* and *copia* served to normalize ChIP-qPCR data.
707 To test if *B'*, *B-I*, *B' mop1-1, B' Mop2/mop2-1*, *B' mop2-1*, *B' mop2-2* and *B' mop3-1*
708 behaved similar for the enrichment of the measured histone modifications in either seedling or
709 husk tissue, two-way Analysis of variance (ANOVA) tests were used. Given the limited
710 sample number, we assumed all datasets to be normally distributed and having similar
711 variances. When the ANOVA tests indicated significant differences between the different
712 (epi)genotypes, a pairwise t-test with a Bonferroni correction for multiple testing was
713 performed to uncover which individual pairs differ significantly. The output from the
714 ANOVAs and pairwise t-tests is summarized in Supplemental Table S2.
715 The *Copia* sequence behaves, on average, as a non-RdDM locus (Parent et al., 2021)
716 and could therefore be used to normalize ChIP-qPCR data obtained for *B' mop1-1* plants. In
717 previous experiments, *Copia* sequences were used to normalize ChIP-qPCR data obtained
718 with antibodies recognizing H3K9me2 and H3K27me2 (Haring et al., 2010, 2007). The
719 majority of *Copia* elements are depleted of siRNAs (Gent et al., 2013), indicating they are
720 rarely targeted by RdDM. To validate that the specific type of *Copia* sequence used in our
721 previous experiments was not targeted by RdDM and could be employed for normalization in
722 *mop* mutant backgrounds, the 107-nt sequence was blasted to the maize B73 genome (version
723 3) using parameters optimized for low similarity (e-value 1e-15) and including low

complexity regions. Of the 163 matches, the 97 that were greater or equal to 95-nt in length, carried at least part of both primer binding sites, and had sequence coverage in a bisulfite sequencing experiment (Gent et al., 2014) were selected. These 97 loci were examined for the presence of CHH methylation, a hallmark of RdDM. Their average CHH methylation level was 1.66%, which is very close to the 1.34% of CHH methylation at non-RdDM loci and significantly different from the average CHH methylation level at RdDM loci (14.51%). In addition, analysis of H3K9me2 data from the same study revealed that these loci had an H3K9me2 enrichment value of 1.10, which is characteristic of non-RdDM loci (H3K9me2 enrichment of 1.12) rather than RdDM loci (H3K9me2 enrichment of 0.55) (Gent et al., 2014). This indicated that our *Copia* control sequence behaves, on average, as a non-RdDM locus and that it could be used to normalize our ChIP-qPCR data obtained from wild-type and *mop* mutant plants.

Chromatin Conformation analysis (3C)

3C analyses were performed on *B' mop1-1* husk tissue as described previously (Louwers et al., 2009a, 2009b). The data for *B' Mop1/Mop1* and *B-I Mop1/Mop1* have been published before (Louwers et al., 2009a) and are shown for comparison. The experiments on *B' mop1-1* tissues were conducted at the same time and using the same methods as the experiments on *B' Mop1/Mop1* and *B-I Mop1/Mop1* tissues. The primers and TaqMan probes used are listed in Louwers *et al.* (2009a) In 3C experiments, to correct for primer amplification efficiencies, for each primer pair the qPCR data was normalized to a random ligation control sample produced using a BAC clone containing the *b1* locus and an amplified control template for the *Sam* locus. To control for quantity and quality of the 3C samples, the data were normalized to 3C values measured for the *Sam* locus.

DNA Methylation Analysis by DNA Blotting

DNA blot analysis was performed as described previously (Haring et al., 2010). Most DNA samples were derived from leaves collected at different stages of development (Supplemental Figures S4, S6 and S7). DNA was isolated (Dellaporta et al., 1983) and 5 µg of DNA was digested with different methylation sensitive restriction enzymes in combination with *Eco*RI or *Bam*HI according to the manufacturer's specifications. After size fractionation by electrophoresis the gels were blotted onto membrane (Blotting-Nylon 66 membranes, Sigma-Aldrich # 15356), followed by UV fixation. The resulting blots were hybridized to a 853-nt repeat probe. The relative band intensities obtained for the enzymes *Hpa*I, *Pst*I, *Hha*I, *Hae*II

758 *Alu*I, *Sau*96I, *Bsm*AI were quantified for all (*Hpa*I, *Hha*I, *Hae*II) or representative examples
759 (*Pst*I, *Alu*I, *Sau*96I, *Bsm*AI), using a Storm 840 phosphorimager and ImageQuant software
760 (GE LifeSciences). The most probable DNA methylation patterns were identified by the least
761 squares fit comparing the relative band intensities with theoretical possible intensities derived
762 from all possible options for DNA methylation patterns (Haring et al., 2010). *Bsm*AI
763 generated relatively small fragments, including similarly sized 5' and 3' border fragments
764 complicating the computational analysis. The degrees of DNA methylation indicated (Figure
765 4A, Supplemental Figure S6, S7) are our best estimates. To test for complete digestion,
766 probes recognizing unmethylated DNA regions at the *b1* locus were used (probes A, D2 and
767 21, Figure 1 in Haring et al., 2010).
768
769 **DNA Methylation Analysis by Bisulfite Sequencing**
770 For bisulfite sequencing, genomic maize DNA was extracted (Dellaporta et al., 1983) from
771 leaf four of two *B'*, two *B-I* and three *B' mop1-1* plants in a V4 stage (Ritchie et al., 1986),
772 and 400 ng of DNA was treated with bisulfite using the EZ DNA Methylation-Gold kit
773 (Zymo Research, D5006). The DNA regions of interest were PCR-amplified (10 min 95°C,
774 followed by 40 PCR cycles (30 sec 95°C, 30 sec 50°C (repeat) or 52°C (*Fie2*), 30 sec 72°C),
775 and 5 min at 72°C). The amplification was performed using MethylTaq DNA polymerase
776 (Diagenode, C09010010), a forward (KL1310; TGGTGTTTAAAAATTYATGTTTTTGTG)
777 and reverse primer (KL1844; TCCACRARTCATCRTCTCCAAACA) for a 320-nt repeat
778 junction fragment and a forward (AAGATTTGAGATTYGATTTGAAGTGTG) and reverse
779 primer (ACTTTCCCCTCCRCCTAATTCTCCTTA) for a 226-nt *Fie2* fragment that served
780 as a control for complete bisulfite conversion (similar to the -302 to -91 fragment described in
781 Gutierrez-Marcos et al., 2006). PCR fragments were cloned into the pJET 1.2 vector
782 (CloneJet PCR Cloning Kit, Thermo Scientific) following the manufacturer's instructions.
783 Clones carrying inserts of the correct size were identified by PCR. DNA was isolated from
784 positive clones (GeneJet Plasmid Miniprep Kit, Thermo scientific) and subjected to Sanger
785 sequencing. To determine the percentage, sequence context and pattern of cytosine
786 methylation, sequences were analyzed using Kismeth (Gruntman et al., 2008). For each DNA
787 sample approximately 15 clones were sequenced for *Fie2*, and 30 clones for the repeat
788 junction region.
789
790 **Genomic Alignments and Data Analysis of DNA methylation-seq and Small RNA Reads**

791 Small RNA sequences from developing ear were obtained from the Sequence Read Archive,
792 runs SRR1583941 and SRR1583942 for the *mop1-1* mutant; and SRR1583943 and
793 SRR1583944 for wild-type (Gent et al., 2014). Both were in a genetic background closely
794 related to B73. The methylC-seq data from the same study were derived from pure B73
795 developing ear, runs SRR1583945, SRR1583946, and SRR1583947. The Enzymatic Methyl-
796 seq (EM-seq) data from developing second leaf of B73 were from the NAM founders
797 assembly project and available through the European Nucleotide Archive, runs ERR5347654,
798 ERR5347655, and ERR5347656 (Hufford et al., 2021).

799 Both methylC-seq and EM-seq reads were processed and mapped with BS-
800 Seeker2 (Guo et al., 2013) according to published methods (Hufford et al., 2021), except that
801 no mismatches were allowed (-m 0) and mapping was done in end-to-end mode (--bt2--end-
802 to-end). Potential PCR duplicates were removed from the ear methylC-seq reads using
803 the BS-Seeker2 FilterReads tool. Methylation values and coverage for genomic loci were
804 obtained using the CGmapTools mtr tool for each of the three sequence contexts separately
805 (Guo et al., 2018). For defining low mCHH and high mCHH *mop1* loci, a minimum effective
806 coverage of 20 was required, where effective coverage is the sum of the read coverage of each
807 individual cytosine in each locus. Methylation values were measured as the average of each
808 site in each locus. Low mCHH *mop1* loci were defined as having less than 0.02 mCHH, and
809 high mCHH *mop1* loci as having greater than or equal to 0.02 mCHH in the source B73 ear
810 methylome (Gent et al., 2014). These were initially identified based on 50-bp non-
811 overlapping intervals, but all adjacent loci that met criteria for low mCHH were merged, and
812 all adjacent loci that met criteria for high mCHH were also merged. Only merged loci
813 consisting of at least two adjacent loci were included in the final sets, giving them minimum
814 lengths of 100 bp. The methylation of these loci was reevaluated using the leaf methylome
815 (Hufford et al., 2021), but with a constraint that only loci with at least five cytosines of the
816 specific cytosine context being spanned by reads were included in the analysis.

817 Small RNA-seq reads were quality filtered, trimmed of adapters, and filtered for
818 lengths of 20-25 nt using cutadapt (Martin, 2011), parameters -q 20 -a
819 AGATCGGAAGAGCACACGTCT -e .05 -O 5 --discard-untrimmed -m 20 -M 25. Reads
820 were aligned to the genome with Bowtie2, –very-sensitive parameters (Langmead and
821 Salzberg, 2012). Reads that overlapped at least 90% of their lengths with tRNA, 5S RNA,
822 NOR, or miRNA loci were removed using the BEDTools intersect tool with parameters -v -f
823 .9 (Quinlan and Hall, 2010). These excluded loci were identified using published methods
824 (Gent et al., 2022), but applied to the B73 v5 reference genome (Hufford et al., 2021). The

825 read counts for miRNA loci were used for normalization in downstream steps. The two input
826 files for wild-type and the two for the *mop1-1* mutant were combined into single files using
827 the SAMtools merge tool (Li et al., 2009) Uniquely-mapping reads were selected using the
828 SAMtools view tool with the -q20 parameter. Perfect-matching siRNAs were selected using
829 grep for the pattern 'NM:i:0'. 24-nt siRNAs were selected from the complete set of 20 to 25-nt
830 siRNAs using grep for the pattern '24M'. Read coverage over 50-bp intervals of the genome
831 was obtained using the BEDTools coverage tool. All intervals were identified that had at least
832 25 overlapping reads and which spanned at least 30 bp of the interval from wild-type. In
833 addition, they had to have a minimum of ten-fold fewer overlapping reads in the *mop1-1*
834 mutant than in wild-type (normalized by the number of miRNA reads). These, called *mop1*
835 loci, were then further filtered using methylation data as to generate low mCHH and high
836 mCHH *mop1* loci as described above.
837
838 **Gene IDs**
839 *mop1*: Zm00001eb080370
840 *mop2/rmr7*: Zm00001eb068960
841 *mop3/rmr6*: Zm00001eb035080
842
843 **Acknowledgements**
844 We would like to thank Vicki Chandler and Lyudmila Sidorenko for providing seeds. We are
845 grateful to Nicole Riddle and Sarah Gadel who tested the specificity of the H3K9me2 and
846 H3K27me2 Cell signaling antibodies with Slot Blots. Shiv Grewal is thanked for advice and
847 fruitful discussion, Ludek Tikovsky and Harold Lemereis for taking excellent care of the
848 maize plants, and Christel Rooker for proofreading of the manuscript. I.H. was supported by
849 the Systems Biology Research Priority fund of the University of Amsterdam. K.P. is
850 supported by the Topsector Horticulture & Starting materials; J.I.G was supported by a
851 National Science Foundation grant (2114797). M.S. was supported by the Royal Netherlands
852 Academy of Arts and Sciences (KNAW).
853
854 **Author contributions**
855 I.H., M.L., M.H., J.I.G. and M.S. designed the research; R.B., I.H., M.L., M.H and J.I.G.
856 performed research, analyzed data and made figures; K.P. performed statistical analysis and
857 generated figures; I.H., J.I.G. and M.S. wrote the manuscript.
858
859 **Supplemental data**

860 **Supplemental Figure S1**. *b1* expression levels in maize husk tissues.

861 **Supplemental Figure S2.** Schematic representation of the *b1* and *Sam* locus.

862 **Supplemental Figure S3.** *B'* hepta-repeat is marked by H3 acetylation in *mop1-1* and *mop3-*
863 *1* mutants.

864 **Supplemental Figure S4.** In *mop* mutants slight differences in DNA methylation were
865 observed at the *B'* repeat junction regions by DNA blot analysis.

866 **Supplemental Figure S5.** Consensus double-stranded DNA sequence of the 2nd-6th repeat.

867 **Supplemental Figure S6.** Detailed DNA methylation data for *B'* in *mop* mutants using
868 methylation sensitive restriction enzymes and DNA blot analysis.

869 **Supplemental Figure S7.** DNA methylation levels at *B'* hepta-repeat do not progressively
870 decrease during development of a *B' mop1-1* plant.

871 **Supplemental Figure S8.** Targeted bisulfite data for *B'*, *B-I*, *B' mop1-1*, *B' Mop2/mop2-1*
872 and *B' mop3-1* DNA derived from leaf 4 of V4 stage plants.

873 **Supplemental Figure S9.** Identification of low and high mCHH *mop1* loci and their
874 respective siRNA levels.

875 **Supplemental Figure S10.** No decrease in nucleosome occupancy was observed in the *mop*
876 mutants.

877 **Supplemental Figure S11.** Transcriptional activation in *mop1-1* and *mop3-1* is associated
878 with reduced levels of repressive histone marks.

879 **Supplemental Table S1.** Primers used in ChIP-qPCR experiments.

880 **Supplemental Table S2.** Statistical analyses of the ChIP-qPCR experiments.

881

882

883 **References**

884 Alleman, M., Sidorenko, L., McGinnis, K., Seshadri, V., Dorweiler, J.E., White, J., Sikkink,
885 K., Chandler, V.L., 2006. An RNA-dependent RNA polymerase is required for
886 paramutation in maize. Nature 442, 295–298. https://doi.org/10.1038/nature04884
887 Arteaga-Vazquez, M., Sidorenko, L., Rabanal, F.A., Shrivistava, R., Nobuta, K., Green, P.J.,
888 Meyers, B.C., Chandler, V.L., 2010. RNA-mediated trans -communication can
889 establish paramutation at the b1 locus in maize. PNAS 107, 12986–12991.
890 https://doi.org/10.1073/pnas.1007972107/-
891 /DCSupplemental.www.pnas.org/cgi/doi/10.1073/pnas.1007972107
892 Bartee, L., Malagnac, F., Bender, J., 2001. Arabidopsis cmt3 chromomethylase mutations
893 block non-CG methylation and silencing of an endogenous gene. Genes Dev 15,
894 1753–1758. https://doi.org/10.1101/gad.905701
895 Belele, C.L., Sidorenko, L., Stam, M., Bader, R., Arteaga-Vazquez, M.A., Chandler, V.L.,
896 2013. Specific Tandem Repeats Are Sufficient for Paramutation-Induced Trans-

897 Generational Silencing. PLoS Genetics 9.
898 https://doi.org/10.1371/journal.pgen.1003773
899 Bernatavichute, Y.V., Zhang, X., Cokus, S., Pellegrini, M., Jacobsen, S.E., 2008. Genome-
900 wide association of histone H3 lysine nine methylation with CHG DNA methylation
901 in Arabidopsis thaliana. PLoS One 3, e3156.
902 https://doi.org/10.1371/journal.pone.0003156
903 Calarco, J.P., Borges, F., Donoghue, M.T.A., Van Ex, F., Jullien, P.E., Lopes, T., Gardner, R.,
904 Berger, F., Feijó, J.A., Becker, J.D., Martienssen, R.A., 2012. Reprogramming of
905 DNA Methylation in Pollen Guides Epigenetic Inheritance via Small RNA. Cell 151,
906 194–205. https://doi.org/10.1016/j.cell.2012.09.001
907 Castel, S.E., Martienssen, R.A., 2013. RNA interference in the nucleus: roles for small RNAs
908 in transcription, epigenetics and beyond. Nat Rev Genet 14, 100–112.
909 https://doi.org/10.1038/nrg3355
910 Conway, E., Healy, E., Bracken, A.P., 2015. PRC2 mediated H3K27 methylations in cellular
911 identity and cancer. Curr Opin Cell Biol 37, 42–48.
912 https://doi.org/10.1016/j.ceb.2015.10.003
913 Dellaporta, S.L., Wood, J., Hicks, J.B., 1983. A plant DNA minipreparation: Version II. Plant
914 Mol Biol Rep 1, 19–21. https://doi.org/10.1007/BF02712670
915 Dorweiler, J.E., Carey, C.C., Kubo, K.M., Hollick, J.B., Kermicle, J.L., Chandler, V.L., 2000.
916 mediator of paramutation1 is required for establishment and maintenance of
917 paramutation at multiple maize loci. Plant Cell 12, 2101–2118.
918 https://doi.org/10.1105/tpc.12.11.2101
919 Du, J., Johnson, L.M., Groth, M., Feng, S., Hale, C.J., Li, S., Vashisht, A.A., Wohlschlegel,
920 J.A., Patel, D.J., Jacobsen, S.E., 2014. Mechanism of DNA methylation-directed
921 histone methylation by KRYPTONITE. Mol Cell 55, 495–504.
922 https://doi.org/10.1016/j.molcel.2014.06.009
923 Du, J., Zhong, X., Bernatavichute, Y.V., Stroud, H., Feng, S., Caro, E., Vashisht, A.A.,
924 Terragni, J., Chin, H.G., Tu, A., Hetzel, J., Wohlschlegel, J.A., Pradhan, S., Patel,
925 D.J., Jacobsen, S.E., 2012. Dual binding of chromomethylase domains to H3K9me2-
926 containing nucleosomes directs DNA methylation in plants. Cell 151, 167–180.
927 https://doi.org/10.1016/j.cell.2012.07.034
928 Egelhofer, T.A., Minoda, A., Klugman, S., Lee, K., Kolasinska-Zwierz, P., Alekseyenko,
929 A.A., Cheung, M.-S., Day, D.S., Gadel, S., Gorchakov, A.A., Gu, T., Kharchenko,
930 P.V., Kuan, S., Latorre, I., Linder-Basso, D., Luu, Y., Ngo, Q., Perry, M.,
931 Rechtsteiner, A., Riddle, N.C., Schwartz, Y.B., Shanower, G.A., Vielle, A., Ahringer,
932 J., Elgin, S.C.R., Kuroda, M.I., Pirrotta, V., Ren, B., Strome, S., Park, P.J., Karpen,
933 G.H., Hawkins, R.D., Lieb, J.D., 2011. An assessment of histone-modification
934 antibody quality. Nat Struct Mol Biol 18, 91–93. https://doi.org/10.1038/nsmb.1972
935 Erhard, K.F., Stonaker, J.L., Parkinson, S.E., Al., E., 2009. RNA Polymerase IV Functions in
936 Paramutation in Zea mays. Science 323, 1201–1205.
937 Ferrari, K.J., Scelfo, A., Jammula, S., Cuomo, A., Barozzi, I., Stützer, A., Fischle, W.,
938 Bonaldi, T., Pasini, D., 2014. Polycomb-dependent H3K27me1 and H3K27me2
939 regulate active transcription and enhancer fidelity. Mol Cell 53, 49–62.
940 https://doi.org/10.1016/j.molcel.2013.10.030
941 Fitz-James, M.H., Cavalli, G., 2022. Molecular mechanisms of transgenerational epigenetic
942 inheritance. Nat Rev Genet 23, 325–341. https://doi.org/10.1038/s41576-021-00438-5
943 Foda, B.M., Singh, U., 2015. Dimethylated H3K27 Is a Repressive Epigenetic Histone Mark
944 in the Protist Entamoeba histolytica and Is Significantly Enriched in Genes Silenced
945 via the RNAi Pathway. Journal of Biological Chemistry 290, 21114–21130.
946 https://doi.org/10.1074/jbc.M115.647263

947 Fu, F.-F., Dawe, R.K., Gent, J.I., 2018. Loss of RNA-Directed DNA Methylation in Maize
948 Chromomethylase and DDM1-Type Nucleosome Remodeler Mutants. The Plant Cell
949 30, 1617–1627. https://doi.org/10.1105/tpc.18.00053
950 Gent, Jonathan I, Ellis, N.A., Guo, L., Harkess, A.E., Yao, Y., Zhang, X., Dawe, R.K., 2013.
951 CHH islands : de novo DNA methylation in near-gene chromatin regulation in maize.
952 Genome research 23, 628–637. https://doi.org/10.1101/gr.146985.112.as
953 Gent, J I, Ellis, N.A., Guo, L., Harkess, A.E., Yao, Y., Zhang, X., Dawe, R.K., 2013. CHH
954 islands: de novo DNA methylation in near-gene chromatin regulation in maize.
955 Genome Research 23, 628–637. https://doi.org/10.1101/gr.146985.112
956 Gent, J.I., Higgins, K.M., Swentowsky, K.W., Fu, F.-F., Zeng, Y., Kim, D.W., Dawe, R.K.,
957 Springer, N.M., Anderson, S.N., 2022. The maize gene maternal derepression of r1
958 encodes a DNA glycosylase that demethylates DNA and reduces siRNA expression in
959 the endosperm. Plant Cell 34, 3685–3701. https://doi.org/10.1093/plcell/koac199
960 Gent, Jonathan I, Madzima, T.F., Bader, R., Kent, M.R., Zhang, X., Stam, M., McGinnis,
961 K.M., Dawe, R.K., 2014b. Accessible DNA and Relative Depletion of H3K9me2 at
962 Maize Loci Undergoing RNA-Directed DNA Methylation. The Plant Cell Online 26,
963 4903–4917. https://doi.org/10.1105/tpc.114.130427
964 Grewal, S.I.S., 2023. The molecular basis of heterochromatin assembly and epigenetic
965 inheritance. Mol Cell 83, 1767–1785. https://doi.org/10.1016/j.molcel.2023.04.020
966 Gruntman, E., Qi, Y., Slotkin, R.K., Roeder, T., Martienssen, R.A., Sachidanandam, R., 2008.
967 Kismeth: Analyzer of plant methylation states through bisulfite sequencing. BMC
968 Bioinformatics 9, 371. https://doi.org/10.1186/1471-2105-9-371
969 Gu, S.G., Pak, J., Guang, S., Maniar, J.M., Kennedy, S., Fire, A., 2012. Amplification of
970 siRNA in Caenorhabditis elegans generates a transgenerational sequence-targeted
971 histone H3 lysine 9 methylation footprint. Nat Genet 44, 157–164.
972 https://doi.org/10.1038/ng.1039
973 Guo, W., Fiziev, P., Yan, W., Cokus, S., Sun, X., Zhang, M.Q., Chen, P.Y., Pellegrini, M.,
974 2013. BS-Seeker2: A versatile aligning pipeline for bisulfite sequencing data. BMC
975 Genomics 14, 1. https://doi.org/10.1186/1471-2164-14-774
976 Guo, W., Zhu, P., Pellegrini, M., Zhang, M.Q., Wang, X., Ni, Z., 2018. CGmapTools
977 improves the precision of heterozygous SNV calls and supports allele-specific
978 methylation detection and visualization in bisulfite-sequencing data. Bioinformatics
979 34, 381–387. https://doi.org/10.1093/bioinformatics/btx595
980 Gutiérrez-Marcos, J.F., Costa, L.M., Dal Prà, M., Scholten, S., Kranz, E., Perez, P.,
981 Dickinson, H.G., 2006. Epigenetic asymmetry of imprinted genes in plant gametes.
982 Nat Genet 38, 876–878. https://doi.org/10.1038/ng1828
983 Haag, J.R., Brower-Toland, B., Krieger, E.K., Sidorenko, L., Nicora, C.D., Norbeck, A.D.,
984 Irsigler, A., LaRue, H., Brzeski, J., McGinnis, K., Ivashuta, S., Pasa-Tolic, L.,
985 Chandler, V.L., Pikaard, C.S., 2014. Functional diversification of maize RNA
986 polymerase IV and V subtypes via alternative catalytic subunits. Cell reports 9, 378–
987 90. https://doi.org/10.1016/j.celrep.2014.08.067
988 Haring, M., Bader, R., Louwers, M., Schwabe, A., van Driel, R., Stam, M., 2010a. The role of
989 DNA methylation, nucleosome occupancy and histone modifications in paramutation.
990 The Plant journal : for cell and molecular biology 63, 366–78.
991 https://doi.org/10.1111/j.1365-313X.2010.04245.x
992 Haring, M., Offermann, S., Danker, T., Horst, I., Peterhansel, C., Stam, M., 2007. Chromatin
993 immunoprecipitation: optimization, quantitative analysis and data normalization. Plant
994 Methods 3, 11. https://doi.org/10.1186/1746-4811-3-11

995 Herr, A.J., Jensen, M.B., Dalmay, T., Baulcombe, D.C., 2005. RNA polymerase IV directs
996 silencing of endogenous DNA. Science 308, 118–120.
997 https://doi.org/10.1126/science.1106910
998 Hollick, J.B., 2017. Paramutation and related phenomena in diverse species. Nat Rev Genet
999 18, 5–23. https://doi.org/10.1038/nrg.2016.115
1000 Hollick, Jay B, Kermicle, J.L., Parkinson, S.E., 2005. Rmr6 maintains meiotic inheritance of
1001 paramutant states in Zea mays. Genetics 171, 725–40.
1002 https://doi.org/10.1534/genetics.105.045260
1003 Hollick, J. B., Kermicle, J.L., Parkinson, S.E., 2005. Rmr6 maintains meiotic inheritance of
1004 paramutant states in Zea mays. Genetics 171, 725–740.
1005 https://doi.org/10.1534/genetics.105.045260
1006 Hollick, J.B., Patterson, G.I., Coe, E.H., Cone, J.K.C., Chandler, V.L., 1995. Allelic
1007 Interactions Heritably Alter the Activity of a Metastable Maize pl Allele. Genetics
1008 141, 709–719.
1009 Hövel, I., Pearson, N.A., Stam, M., 2015. Cis-acting determinants of paramutation. Semin
1010 Cell Dev Biol 44, 22–32. https://doi.org/10.1016/j.semcdb.2015.08.012
1011 Hufford, M.B., Seetharam, A.S., Woodhouse, M.R., Chougule, K.M., Ou, S., Liu, J., Ricci,
1012 W.A., Guo, T., Olson, A., Qiu, Y., Della Coletta, R., Tittes, S., Hudson, A.I., Marand,
1013 A.P., Wei, S., Lu, Z., Wang, B., Tello-Ruiz, M.K., Piri, R.D., Wang, N., Kim, D.W.,
1014 Zeng, Y., O'Connor, C.H., Li, X., Gilbert, A.M., Baggs, E., Krasileva, K.V.,
1015 Portwood, J.L., Cannon, E.K.S., Andorf, C.M., Manchanda, N., Snodgrass, S.J.,
1016 Hufnagel, D.E., Jiang, Q., Pedersen, S., Syring, M.L., Kudrna, D.A., Llaca, V.,
1017 Fengler, K., Schmitz, R.J., Ross-Ibarra, J., Yu, J., Gent, J.I., Hirsch, C.N., Ware, D.,
1018 Dawe, R.K., 2021. De novo assembly, annotation, and comparative analysis of 26
1019 diverse maize genomes. Science 373, 655–662.
1020 https://doi.org/10.1126/science.abg5289
1021 Jackel, J.N., Storer, J.M., Coursey, T., Bisaro, D.M., 2016. Arabidopsis RNA Polymerases IV
1022 and V Are Required To Establish H3K9 Methylation, but Not Cytosine Methylation,
1023 on Geminivirus Chromatin. Journal of Virology 90, 7529–7540.
1024 https://doi.org/10.1128/jvi.00656-16
1025 Jia, Y., Lisch, D.R., Ohtsu, K., Scanlon, M.J., Nettleton, D., Schnable, P.S., 2009. Loss of
1026 RNA-dependent RNA polymerase 2 (RDR2) function causes widespread and
1027 unexpected changes in the expression of transposons, genes, and 24-nt small RNAs.
1028 PLoS Genet 5, e1000737. https://doi.org/10.1371/journal.pgen.1000737
1029 Jiang, C., Pugh, B.F., 2009. Nucleosome positioning and gene regulation: advances through
1030 genomics. Nat Rev Genet 10, 161–172. https://doi.org/10.1038/nrg2522
1031 Johnson, L.M., Bostick, M., Zhang, X., Kraft, E., Henderson, I., Callis, J., Jacobsen, S.E.,
1032 2007. The SRA methyl-cytosine-binding domain links DNA and histone methylation.
1033 Curr Biol 17, 379–384. https://doi.org/10.1016/j.cub.2007.01.009
1034 Kanno, T., Huettel, B., Mette, M.F., Aufsatz, W., Jaligot, E., Daxinger, L., Kreil, D.P.,
1035 Matzke, M., Matzke, A.J.M., 2005. Atypical RNA polymerase subunits required for
1036 RNA-directed DNA methylation. Nat Genet 37, 761–765.
1037 https://doi.org/10.1038/ng1580
1038 Langmead, B., Salzberg, S.L., 2012. Fast gapped-read alignment with Bowtie 2. Nat Methods
1039 9, 357–359. https://doi.org/10.1038/nmeth.1923
1040 Law, J.A., Vashisht, A.A., Wohlschlegel, J.A., Jacobsen, S.E., 2011. SHH1, a homeodomain
1041 protein required for DNA methylation, as well as RDR2, RDM4, and chromatin
1042 remodeling factors, associate with RNA polymerase IV. PLoS Genet 7, e1002195.
1043 https://doi.org/10.1371/journal.pgen.1002195

1044 Lee, H.-G., Kahn, T.G., Simcox, A., Schwartz, Y.B., Pirrotta, V., 2015. Genome-wide
1045 activities of Polycomb complexes control pervasive transcription. Genome Res. 25,
1046 1170–1181. https://doi.org/10.1101/gr.188920.114
1047 Li, H., Handsaker, B., Wysoker, A., Fennell, T., Ruan, J., Homer, N., Marth, G., Abecasis, G.,
1048 Durbin, R., 1000 Genome Project Data Processing Subgroup, 2009. The Sequence
1049 Alignment/Map format and SAMtools. Bioinformatics 25, 2078–2079.
1050 https://doi.org/10.1093/bioinformatics/btp352
1051 Li, Q., Eichten, S.R., Hermanson, P.J., Zaunbrecher, V.M., Song, J., Wendt, J., Rosenbaum,
1052 H., Madzima, T.F., Sloan, A.E., Huang, J., Burgess, D.L., Richmond, T.A., McGinnis,
1053 K.M., Meeley, R.B., Danilevskaya, O.N., Vaughn, M.W., Kaeppler, S.M., Jeddeloh,
1054 J.A., Springer, N.M., 2014. Genetic Perturbation of the Maize Methylome. The Plant
1055 Cell Online 26, 4602–4616. https://doi.org/10.1105/tpc.114.133140
1056 Li, Q., Gent, J.I., Zynda, G., Song, J., Makarevitch, I., Hirsch, C.D., Hirsch, C.N., Dawe,
1057 R.K., Madzima, T.F., McGinnis, K.M., Lisch, D., Schmitz, R.J., Vaughn, M.W.,
1058 Springer, N.M., 2015. RNA-directed DNA methylation enforces boundaries between
1059 heterochromatin and euchromatin in the maize genome. Proceedings of the National
1060 Academy of Sciences 112, 14728–14733. https://doi.org/10.1073/pnas.1514680112
1061 Lindroth, A.M., Cao, X., Jackson, J.P., Zilberman, D., McCallum, C.M., Henikoff, S.,
1062 Jacobsen, S.E., 2001. Requirement of CHROMOMETHYLASE3 for maintenance of
1063 CpXpG methylation. Science 292, 2077–2080.
1064 https://doi.org/10.1126/science.1059745
1065 Liu, Y., Taverna, S.D., Muratore, T.L., Shabanowitz, J., Hunt, D.F., Allis, C.D., 2007. RNAi-
1066 dependent H3K27 methylation is required for heterochromatin formation and DNA
1067 elimination in Tetrahymena. Genes Dev 21, 1530–1545.
1068 https://doi.org/10.1101/gad.1544207
1069 Liu, Y., Yuan, J., Jia, G., Ye, W., Jeffrey Chen, Z., Song, Q., 2021. Histone H3K27
1070 dimethylation landscapes contribute to genome stability and genetic recombination
1071 during wheat polyploidization. The Plant Journal 105, 678–690.
1072 https://doi.org/10.1111/tpj.15063
1073 Locatelli, S., Piatti, P., Motto, M., Rossi, V., 2009. Chromatin and DNA modifications in the
1074 Opaque2-mediated regulation of gene transcription during maize endosperm
1075 development. Plant Cell 21, 1410–1427. https://doi.org/10.1105/tpc.109.067256
1076 Louwers, M., Bader, R., Haring, M., van Driel, R., de Laat, W., Stam, M., 2009a. Tissue- and
1077 expression level-specific chromatin looping at maize b1 epialleles. The Plant Cell 21,
1078 832–42. https://doi.org/10.1105/tpc.108.064329
1079 Louwers, M., Splinter, E., van Driel, R., de Laat, W., Stam, M., 2009b. Studying physical
1080 chromatin interactions in plants using Chromosome Conformation Capture (3C). Nat
1081 Protoc 4, 1216–1229. https://doi.org/10.1038/nprot.2009.113
1082 Martin, M., 2011. Cutadapt removes adapter sequences from high-throughput sequencing
1083 reads. EMBnet.journal 17, 10–12. https://doi.org/10.14806/ej.17.1.200
1084 Mathieu, O., Probst, A.V., Paszkowski, J., 2005. Distinct regulation of histone H3
1085 methylation at lysines 27 and 9 by CpG methylation in Arabidopsis. The EMBO
1086 Journal 24, 2783–2791. https://doi.org/10.1038/sj.emboj.7600743
1087 Mathieu, O., Reinders, J., Caikovski, M., Smathajitt, C., Paszkowski, J., 2007.
1088 Transgenerational stability of the Arabidopsis epigenome is coordinated by CG
1089 methylation. Cell 130, 851–862. https://doi.org/10.1016/j.cell.2007.07.007
1090 Matzke, M.A., Mosher, R.A., 2014. RNA-directed DNA methylation: an epigenetic pathway
1091 of increasing complexity. Nat Rev Genet 15, 394–408.
1092 https://doi.org/10.1038/nrg3683

1093 Mishra, V., Singh, J., Wang, F., Zhang, Y., Fukudome, A., Trinidad, J.C., Takagi, Y.,
1094 Pikaard, C.S., 2021. Assembly of a dsRNA synthesizing complex: RNA-
1095 DEPENDENT RNA POLYMERASE 2 contacts the largest subunit of NUCLEAR
1096 RNA POLYMERASE IV. Proc Natl Acad Sci U S A 118, e2019276118.
1097 https://doi.org/10.1073/pnas.2019276118
1098 Nobuta, K., Lu, C., Shrivastava, R., Pillay, M., De Paoli, E., Accerbi, M., Arteaga-Vazquez,
1099 M., Sidorenko, L., Jeong, D.-H., Yen, Y., Green, P.J., Chandler, V.L., Meyers, B.C.,
1100 2008a. Distinct size distribution of endogeneous siRNAs in maize: Evidence from
1101 deep sequencing in the mop1-1 mutant. Proc Natl Acad Sci U S A 105, 14958–14963.
1102 https://doi.org/10.1073/pnas.0808066105
1103 Nobuta, K., Lu, C., Shrivastava, R., Pillay, M., Paoli, E. De, Accerbi, M., Arteaga-vazquez,
1104 M., Sidorenko, L., Jeong, D., Yen, Y., Green, P.J., Chandler, V.L., Meyers, B.C.,
1105 2008b. Distinct size distribution of endogenous siRNAs in maize : Evidence from
1106 deep sequencing in the mop1-1 mutant. PNAS 105, 14958–14963.
1107 Ohtsu, K., Smith, M.B., Emrich, S.J., Borsuk, L.A., Zhou, R., Chen, T., Zhang, X.,
1108 Timmermans, M.C.P., Beck, J., Buckner, B., Janick-Buckner, D., Nettleton, D.,
1109 Scanlon, M.J., Schnable, P.S., 2007. Global gene expression analysis of the shoot
1110 apical meristem of maize (Zea mays L.). Plant J 52, 391–404.
1111 https://doi.org/10.1111/j.1365-313X.2007.03244.x
1112 Onodera, Y., Haag, J.R., Ream, T., Costa Nunes, P., Pontes, O., Pikaard, C.S., 2005. Plant
1113 nuclear RNA polymerase IV mediates siRNA and DNA methylation-dependent
1114 heterochromatin formation. Cell 120, 613–622.
1115 https://doi.org/10.1016/j.cell.2005.02.007
1116 Pal-Bhadra, M., Leibovitch, B.A., Gandhi, S.G., Rao, M., Bhadra, U., Birchler, J.A., Elgin,
1117 S.C.R., 2004. Heterochromatic Silencing and HP1 Localization in Drosophila Are
1118 Dependent on the RNAi Machinery. Science 303, 669–672.
1119 https://doi.org/10.1126/science.1092653
1120 Papa, C.M., Springer, N.M., Muszynski, M.G., Meeley, R., Kaeppler, S.M., 2001. Maize
1121 chromomethylase Zea methyltransferase2 is required for CpNpG methylation. Plant
1122 Cell 13, 1919–1928. https://doi.org/10.1105/tpc.010064
1123 Parent, J.-S., Cahn, J., Herridge, R.P., Grimanelli, D., Martienssen, R.A., 2021. Small RNAs
1124 guide histone methylation in Arabidopsis embryos. Genes Dev. 35, 841–846.
1125 https://doi.org/10.1101/gad.343871.120
1126 Park, S., Oh, S., Nocker, S. van, 2012. Genomic and Gene-Level Distribution of Histone H3
1127 Dimethyl Lysine-27 (H3K27me2) in Arabidopsis. PLOS ONE 7, e52855.
1128 https://doi.org/10.1371/journal.pone.0052855
1129 Patterson, G.I., Thorpe, C.J., Chandler, V.L., 1993. Paramutation, an allelic interaction, is
1130 associated with a stable and heritable reduction of transcription of the maize b
1131 regulatory gene. Genetics 135, 881–894. https://doi.org/10.1093/genetics/135.3.881
1132 Plank, J.L., Dean, A., 2014. Enhancer function: mechanistic and genome-wide insights come
1133 together. Mol Cell 55, 5–14. https://doi.org/10.1016/j.molcel.2014.06.015
1134 Pontier, D., Yahubyan, G., Vega, D., Bulski, A., Saez-Vasquez, J., Hakimi, M.-A., Lerbs-
1135 Mache, S., Colot, V., Lagrange, T., 2005. Reinforcement of silencing at transposons
1136 and highly repeated sequences requires the concerted action of two distinct RNA
1137 polymerases IV in Arabidopsis. Genes Dev 19, 2030–2040.
1138 https://doi.org/10.1101/gad.348405
1139 Quinlan, A.R., Hall, I.M., 2010. BEDTools: a flexible suite of utilities for comparing genomic
1140 features. Bioinformatics 26, 841–842. https://doi.org/10.1093/bioinformatics/btq033
1141 Ritchie, S.W., Hanway, J.J., Benson, G.O., 1986. How a corn plant develops, 1986
1142 (Departmental Report).

1143 Ronsseray, S., 2015. Paramutation phenomena in non-vertebrate animals. Semin Cell Dev
1144 Biol 44, 39–46. https://doi.org/10.1016/j.semcdb.2015.08.009
1145 Roudier, F., Ahmed, I., Bérard, C., Sarazin, A., Mary-Huard, T., Cortijo, S., Bouyer, D.,
1146 Caillieux, E., Duvernois-Berthet, E., Al-Shikhley, L., Giraut, L., Després, B.,
1147 Drevensek, S., Barneche, F., Dèrozier, S., Brunaud, V., Aubourg, S., Schnittger, A.,
1148 Bowler, C., Martin-Magniette, M.-L., Robin, S., Caboche, M., Colot, V., 2011.
1149 Integrative epigenomic mapping defines four main chromatin states in Arabidopsis:
1150 Organization of the Arabidopsis epigenome. The EMBO Journal 30, 1928–1938.
1151 https://doi.org/10.1038/emboj.2011.103
1152 Rymen, B., Ferrafiat, L., Blevins, T., 2020. Non-coding RNA polymerases that silence
1153 transposable elements and reprogram gene expression in plants. Transcription 11,
1154 172–191. https://doi.org/10.1080/21541264.2020.1825906
1155 Schmitz, R.J., Grotewold, E., Stam, M., 2022. Cis-regulatory sequences in plants: Their
1156 importance, discovery, and future challenges. Plant Cell 34, 718–741.
1157 https://doi.org/10.1093/plcell/koab281
1158 Sekhon, R.S., Lin, H., Childs, K.L., Hansey, C.N., Buell, C.R., de Leon, N., Kaeppler, S.M.,
1159 2011. Genome-wide atlas of transcription during maize development. Plant J 66, 553–
1160 563. https://doi.org/10.1111/j.1365-313X.2011.04527.x
1161 Sekhon, R.S., Wang, P.-H., Sidorenko, L., Chandler, V.L., Chopra, S., 2012. Maize Unstable
1162 factor for orange1 is required for maintaining silencing associated with paramutation
1163 at the pericarp color1 and booster1 loci. PLoS Genet 8, e1002980.
1164 https://doi.org/10.1371/journal.pgen.1002980
1165 Sidorenko, L., Chandler, V., 2008. RNA-dependent RNA polymerase is required for
1166 enhancer-mediated transcriptional silencing associated with paramutation at the maize
1167 p1 gene. Genetics 180, 1983–1993. https://doi.org/10.1534/genetics.108.095281
1168 Sidorenko, L., Dorweiler, J.E., Cigan, a M., Arteaga-Vazquez, M., Vyas, M., Kermicle, J.,
1169 Jurcin, D., Brzeski, J., Cai, Y., Chandler, V.L., 2009. A dominant mutation in
1170 mediator of paramutation2, one of three second-largest subunits of a plant-specific
1171 RNA polymerase, disrupts multiple siRNA silencing processes. PLoS genetics 5,
1172 e1000725. https://doi.org/10.1371/journal.pgen.1000725
1173 Sloan, Amy E., Sidorenko, L., McGinnis, K.M., 2014. Diverse gene-silencing mechanisms
1174 with distinct requirements for RNA polymerase subunits in Zea mays. Genetics 198,
1175 1031–1042. https://doi.org/10.1534/genetics.114.168518
1176 Springer, N.M., McGinnis, K.M., 2015. Paramutation in evolution, population genetics and
1177 breeding. Semin Cell Dev Biol 44, 33–38.
1178 https://doi.org/10.1016/j.semcdb.2015.08.010
1179 Stam, M., Belele, C., Dorweiler, J.E., Chandler, V.L., 2002a. Differential chromatin structure
1180 within a tandem array 100 kb upstream of the maize b1 locus is associated with
1181 paramutation. Genes and Development 16, 1906–1918.
1182 https://doi.org/10.1101/gad.1006702
1183 Stam, M., Belele, C., Ramakrishna, W., Dorweiler, J.E., Bennetzen, J.L., Chandler, V.L.,
1184 2002b. The regulatory regions required for B' paramutation and expression are located
1185 far upstream of the maize b1 transcribed sequences. Genetics 162, 917–930.
1186 https://doi.org/10.1093/genetics/162.2.917
1187 Stonaker, Jennifer L., Lim, J.P., Erhard, K.F., Hollick, J.B., 2009. Diversity of Pol IV
1188 function is defined by mutations at the maize rmr7 locus. PLoS Genet 5, e1000706.
1189 https://doi.org/10.1371/journal.pgen.1000706
1190 Stroud, H., Do, T., Du, J., Zhong, X., Feng, S., Johnson, L., Patel, D.J., Jacobsen, S.E., 2014.
1191 Non-CG methylation patterns shape the epigenetic landscape in Arabidopsis. Nat
1192 Struct Mol Biol 21, 64–72. https://doi.org/10.1038/nsmb.2735

1193 Stroud, H., Greenberg, M.V.C., Feng, S., Bernatavichute, Y.V., Jacobsen, S.E., 2013.
1194 Comprehensive analysis of silencing mutants reveals complex regulation of the
1195 Arabidopsis methylome. Cell 152, 352–364. https://doi.org/10.1016/j.cell.2012.10.054
1196 Struhl, K., Segal, E., 2013. Determinants of nucleosome positioning. Nat Struct Mol Biol 20,
1197 267–273. https://doi.org/10.1038/nsmb.2506
1198 Tang, K., Lang, Z., Zhang, H., Zhu, J.-K., 2016. The DNA demethylase ROS1 targets
1199 genomic regions with distinct chromatin modifications. Nat Plants 2, 16169.
1200 https://doi.org/10.1038/nplants.2016.169
1201 Underwood, C.J., Choi, K., Lambing, C., Zhao, X., Serra, H., Borges, F., Simorowski, J.,
1202 Ernst, E., Jacob, Y., Henderson, I.R., Martienssen, R.A., 2018. Epigenetic activation
1203 of meiotic recombination near Arabidopsis thaliana centromeres via loss of H3K9me2
1204 and non-CG DNA methylation. Genome Res 28, 519–531.
1205 https://doi.org/10.1101/gr.227116.117
1206 Verdel, A., Jia, S., Gerber, S., Sugiyama, T., Gygi, S., Grewal, S.I.S., Moazed, D., 2004.
1207 RNAi-mediated targeting of heterochromatin by the RITS complex. Science 303,
1208 672–676. https://doi.org/10.1126/science.1093686
1209 West, P.T., Li, Q., Ji, L., Eichten, S.R., Song, J., Vaughn, M.W., Schmitz, R.J., Springer,
1210 N.M., 2014. Genomic distribution of H3K9me2 and DNA methylation in a maize
1211 genome. PLoS One 9, e105267. https://doi.org/10.1371/journal.pone.0105267
1212 Wierzbicki, A.T., Haag, J.R., Pikaard, C.S., 2008. Noncoding transcription by RNA
1213 polymerase Pol IVb/Pol V mediates transcriptional silencing of overlapping and
1214 adjacent genes. Cell 135, 635–648. https://doi.org/10.1016/j.cell.2008.09.035
1215 Woodhouse, M.R., Freeling, M., Lisch, D., 2006a. Initiation, establishment, and maintenance
1216 of heritable MuDR transposon silencing in maize are mediated by distinct factors.
1217 PLoS Biol 4, e339. https://doi.org/10.1371/journal.pbio.0040339
1218 Woodhouse, M.R., Freeling, M., Lisch, D., 2006b. The mop1 (mediator of paramutation1)
1219 mutant progressively reactivates one of the two genes encoded by the MuDR
1220 transposon in maize. Genetics 172, 579–592.
1221 https://doi.org/10.1534/genetics.105.051383
1222 Xie, W., Schultz, M.D., Lister, R., Hou, Z., Rajagopal, N., Ray, P., Whitaker, J.W., Tian, S.,
1223 Hawkins, R.D., Leung, D., Yang, H., Wang, T., Lee, A.Y., Swanson, S.A., Zhang, J.,
1224 Zhu, Y., Kim, A., Nery, J.R., Urich, M.A., Kuan, S., Yen, C., Klugman, S., Yu, P.,
1225 Suknuntha, K., Propson, N.E., Chen, H., Edsall, L.E., Wagner, U., Li, Y., Ye, Z.,
1226 Kulkarni, A., Xuan, Z., Chung, W.-Y., Chi, N.C., Antosiewicz-Bourget, J.E., Slukvin,
1227 I., Stewart, R., Zhang, M.Q., Wang, W., Thomson, J.A., Ecker, J.R., Ren, B., 2013.
1228 Epigenomic analysis of multilineage differentiation of human embryonic stem cells.
1229 Cell 153, 1134–1148. https://doi.org/10.1016/j.cell.2013.04.022
1230 Zemach, A., Kim, M.Y., Hsieh, P.-H., Coleman-Derr, D., Eshed-Williams, L., Thao, K.,
1231 Harmer, S.L., Zilberman, D., 2013. The Arabidopsis Nucleosome Remodeler DDM1
1232 Allows DNA Methyltransferases to Access H1-Containing Heterochromatin. Cell 153,
1233 193–205. https://doi.org/10.1016/j.cell.2013.02.033
1234 Zofall, M., Sandhu, R., Holla, S., Wheeler, D., Grewal, S.I.S., 2022. Histone deacetylation
1235 primes self-propagation of heterochromatin domains to promote epigenetic
1236 inheritance. Nat Struct Mol Biol 29, 898–909. https://doi.org/10.1038/s41594-022-
1237 00830-7
1238
1239
1240
1241

1242

1243 **Table S1. Primers used in ChIP-qPCR experiments.**

Gene	Primer set	Sequence	Position relative to TSS	Primer name
b1	5'R	5' CTC GGG GTC AAA TGG ACG G 3'	107.0 kb upstream Fw	M85
		5' GCG GTC ACA ACC TTT TCA GAT C 3'	106.9 kb upstream Rv	M317
	R1	5' GGT TTG CTG CAT CCT TGA CC 3'	~ 100 kb upstream Fw	M12
		5' CTG CAC AGG CTG CAG CAG 3'	~ 100 kb upstream Rv	M295
	R2	5'-GTG GAC AAA TAG TGC ATT CAC CTC AC-3'	~ 100 kb upstream Fw	M111
		5'-GAA ACT GAA CTA ACC AAT GTG GCT-3'	~ 100 kb upstream Rv	M296
	R3	5'-CAA GAT CCA TTG AAC ATC TTG TCC-3'	~ 100 kb upstream Fw	M297
		5'-CAT GTG TGA GGG TGA TGC TGC G-3'	~ 100 kb upstream Rv	M10
	R4	5'-CTA TGC TCG TGC GAA GGG TGG TC-3'	~ 100 kb upstream Fw	M11
		5'-CAG ATC CCC TAT CTA ATC CCA TGT-3'	~ 100 kb upstream Rv	M298
	R5	5'-GCG GGT GAC CAG TGT TT-3'	~ 100 kb upstream Fw	M668
		5'-GAC CTC TTG GAG CCC TCT AAT TTG-3'	~ 100 kb upstream Rv	M669
	R6	5'-CAA ATT AGA GGG CTC CAA GAG GTC-3'	~ 100 kb upstream Fw	M112
		5'-GTT GTG TAC TGC AGT GTT AGG TAG-3'	~ 100 kb upstream Rv	M15
	e	5' CTG GCG GCA CTA AAA AAC G 3'	45.3 kb upstream Fw	M975
		5' TGT GCC CAC CTT TAT TGT GAG TT 3'	45.2 kb upstream Rv	M976
	h	5' ACC AGT CCA ACC TAG CTT GGA AT 3'	41.9 kb upstream Fw	M611
		5' GTC ATT GCG TGC GGC TAT C 3'	41.8 kb upstream Rv	M334
	l	5' TCC ATC TCA CCT CTC ATT GTA TCT TT 3'	8.6 kb upstream Fw	M984
		5' AAA TCG TGT ATA TGG TCG TTT AAA ACA T 3'	8.5 kb upstream Rv	M985
	5'b	5'-GGT GTG CAC ACC ATT AAT TGA-3'	1.2 kb upstream Fw	M119
		5'-CGA TAT TTT GGT GAA AAC TGT TC-3'	1.0 kb upstream Rv	M102
	UTR	5' CTC TTC TGA TCT TCT TCA CCG TCT C 3'	0.4 kb downstream Fw	M108
		5' ATT CCC GGG CGG CCG CGC CTT ACT AAT CCT TC 3'	0.5 kb downstream Rv	M44
	Ex3	5' ACC AGC TGC TCA TGC AGA GGA 3'	1.3 kb downstream Fw	M120
		5' AGG AAG GCG TAG GTC ATG CAG AT 3'	1.4 kb downstream Rv	M121
Actin		5'-GGT GTG CAC ACC ATT AAT TGA-3'	coding region of Actin	M70
		5'-CAC TTT CTG CTC ATG GTT TAA GG-3'	coding region of Actin	M414
Copia		5'-CGA TGT GAA GAC AGC ATT CCT-3'	coding region of Copia	M688
		5'-CTC AAG TGA CAT CCC ATG TGT-3'	coding region of Copia	M689

1244
1245

1246 **Figure legends**

1247 **Figure 1.** *b1* expression levels in maize husk tissues. RNA blot analysis of RNA from *B'*, *B-I*
1248 and *B' mop1-1, B' Mop2/mop2-1, B' mop3-1* husk tissue, using probes recognizing the coding
1249 region of *b1* (exons 7-9) and *Sam* (see Supplemental Figure S2B). The intensities of the bands
1250 representing full-length transcripts were quantified. The indicated values represent the
1251 average plus standard deviation of *b1* transcript levels normalized to *Sam* transcript levels.

1252

1253 **Figure 2.** The regulatory hepta-repeat is activated in *mop1-1* and *mop3-1*, but not in *mop2*
1254 mutants. A) Schematic representation of the *b1* locus including coding region (white box) and
1255 hepta-repeat enhancer (arrowheads). Regions monitored in ChIP are indicated below in green.
1256 The fragments (I-XII) examined by 3C (see Figure 3) are indicated as dark grey boxes. B)
1257 ChIP-qPCR experiments were performed on husk tissue from *B'*, *B' mop1-1*, *B' Mop*/*mop2-1*,
1258 *B' mop2-1*, *B' mop3-1* and *B-I* plants with an antibody recognizing H3ac. ChIP signals were
1259 normalized to *actin* ChIP signals. Error bars indicate standard error of the mean (SEM) of
1260 three *(B'*, *B' mop1-1*, *B' Mop*/*mop2-1)*, or four (*B' mop2-1*, *B' mop3-I, B-I)* biological
1261 replicates. See Supplemental Table S2 for summary of ChIP statistics.

1262

1263 **Figure 3.** *B'* shows a multi-loop structure in the *mop1-1* and *mop3-1* mutant background, and
1264 a single loop structure in *Mop2/mop2-1* mutant background. At the top a schematic
1265 representation of the *b1* locus including the coding region (white box) and hepta-repeat
1266 enhancer (arrowheads). The *Bgl*II fragments (I-XII) examined by 3C are indicated as dark
1267 grey boxes. The viewpoints I (TSS; panel A), X (Hepta-repeat; panel B), and VII (~47kb
1268 upstream; panel C) are indicated by black vertical bars. Data were normalized using
1269 crosslinking frequencies measured for the *Sam* locus (Supplementary Figure S2). Error bars
1270 indicate the SEM of four biological replicates each for *B' mop1-1*, *B' Mop2/mop2-1* and *B'*
1271 *mop3-1*. Data for *B'* and *B-I* (reproduced from Louwers et al., 2009) are shown in shading for
1272 comparison. The experiments for *B'*, *B-I*, and the *mop* mutants were done in parallel.

1273

1274 **Figure 4.** Differentially methylated repeat junction region retains high levels of symmetric
1275 DNA methylation in *mop* mutants. A) Summary of the DNA methylation levels data obtained
1276 by DNA blot analysis. DNA derived from *B'* wild type, *B-I* and *B' mop* mutants was digested
1277 with the methylation-insensitive *Eco*RI or *Bam*HI and the methylation-sensitive enzymes
1278 indicated. A zoom of part of the hepta-repeat, spanning the repeat junction region, is shown.
1279 The consensus repeat methylation profiles of *B'* and *B-I* (Haring et al., 2010) are shown. DNA

1280 methylation levels are specified by colors: 0-12.5%, white; 12.5-37.5%, yellow; 37.5-62.5%,
1281 orange; 62.5-87.5%, red; 87.5-100% methylation, dark red. H, *Hpa*I; P, *Pst*I; E, *Hha*I and
1282 *Hae*II; A, *Alu*I; S, *Sau*96I; U, *Sau*3AI; B, *Bsm*AI; Numbers discriminate individual sites
1283 present more than once every repeat. For details on the quantification of the DNA methylation
1284 levels see Haring *et al.* (2010). B) DNA methylation profiles of the *b1* repeat junction region
1285 at base-pair resolution for *B'* and *B-I*, generated by targeted bisulfite sequencing. This region
1286 includes the R1 and R6 loci assayed by ChIP-qPCR. See Supplementary Fig. S8 for all data
1287 sets. The dot-plots show the DNA methylation for 30 and 31 individual *B'* and *B-I* clones,
1288 respectively. Methylated and unmethylated cytosines are represented by filled and empty
1289 circles, respectively. Red, CG; Blue, CHG; Green, CHH. The restriction sites examined by
1290 DNA blotting are indicated above the panel for comparison. E indicates a site cut by both
1291 *Hha*I and *Hae*II. C) Total fraction of methylated cytosines in the repeat junction region in all
1292 three sequence contexts as measured by bisulfite sequencing. The mean and standard
1293 deviations shown are calculated from three (*B' mop1-1*) or two (all other genotypes)
1294 biological replicates. *M/mop2* indicates *Mop2/mop2-1.*
1295
1296 **Figure 5.** The maize genome contains low-mCHH and high-mCHH RdDM loci. Average
1297 DNA methylation levels for high and low mCHH loci in the developing second leaf of B73.
1298 Values of 5-methylcytosine are relative to the total number of cytosines (mC/total C) in each
1299 sequence context (CG, CHG, or CHH).
1300
1301 **Figure 6.** No significant decrease in nucleosome occupancy was observed in the *mop*
1302 mutants. ChIP experiments were performed with an antibody recognizing histone H3, using
1303 husk tissue from *B'* (light green), *B' Mop*/*mop2-1* (green), *B' mop2-1* (black), *B' mop1-1*
1304 (magenta)*, B' mop3-1* (blue), and *B-I* (purple) plants. Data was normalized to *actin* values.
1305 The error bars indicate the standard error of the mean (SEM) of two (*B' mop1-1*), three (*B'*,
1306 *B' Mop*/*mop2-1*, *B' mop3-1),* or four (*B' mop2-1*, *B-I*) replicate experiments. For the no-
1307 antibody control signals see Supplemental Figure S10.
1308
1309 **Figure 7.** Transcriptional activation in *mop1-1* and *mop3-1* is associated with reduced levels
1310 of repressive histone marks. ChIP-qPCR experiments were performed on seedling (A, C) and
1311 husk tissue (B, D) from *B'*, *B' Mop*/*mop2-1*, *B' mop2-1*, *B' mop1-1*, *B' mop3-1* and *B-I* plants
1312 with antibodies recognizing H3K9me2 (A, B), and H3K27me2 (C, D). ChIP signals were
1313 normalized to *Copia* signals. Error bars indicate the SEM of multiple biological replicates.

1314 For seedlings, three (*B'*, *B' mop1-1*) or two (*B' mop3-1, B-I)* replicates were performed. For
1315 husks (B, D), two (*B' mop2-2*), three (*B', B' mop3-1*, *B-I*), four (*B' mop1-1, B' Mop*/*mop2-1*,
1316 *B' mop2-1)* replicates were performed. For the no-antibody control signals see Supplemental
1317 Figure S11.
1318

Figure 1

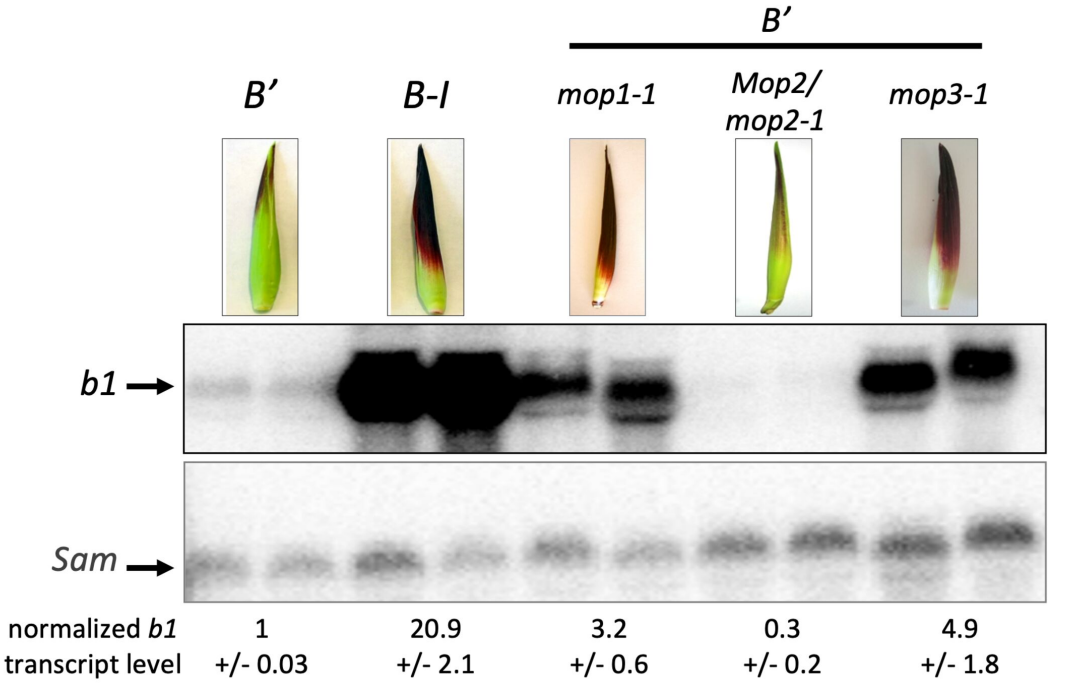

Figure 1. *b1* expression levels in maize husk tissues. RNA blot analysis of RNA from *B'*, *B-I* and *B' mop1-1, B' Mop2/mop2-1, B' mop3-1* husk tissue, using probes recognizing the coding region of *b1* (exons 7-9) and *Sam* (see Supplemental Figure S2B). The intensities of the bands representing full-length transcripts were quantified. The indicated values represent the average plus standard deviation of *b1* transcript levels normalized to *Sam* transcript levels.

Figure 2

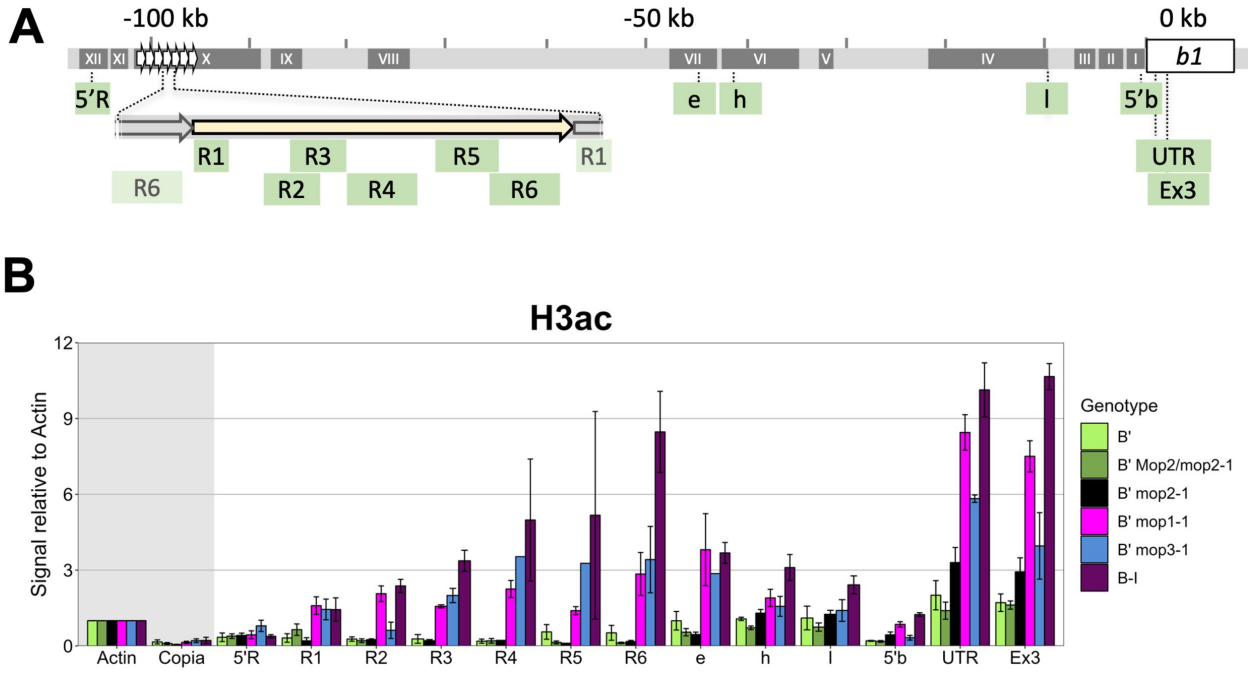

Figure 2. The regulatory hepta-repeat is activated in *mop1-1* and *mop3-1*, but not in *mop2* mutants. A) Schematic representation of the *b1* locus including coding region (white box) and hepta-repeat enhancer (arrowheads). Regions monitored in ChIP are indicated below in green. The fragments (I-XII) examined by 3C (see Figure 3) are indicated as dark grey boxes. B) ChIP-qPCR experiments were performed on husk tissue from *B'*, *B' mop1-1*, *B' Mop/mop2-1*, *B' mop2-1*, *B' mop3-1* and *B-I* plants with an antibody recognizing H3ac. ChIP signals were normalized to *actin* ChIP signals. Error bars indicate standard error of the mean (SEM) of three *(B'*, *B' mop1-1*, *B' Mop/mop2-1)*, or four (*B' mop2-1*, *B' mop3-I, B-I)* biological replicates. See Supplemental Table S2 for summary of ChIP statistics.

Figure 3

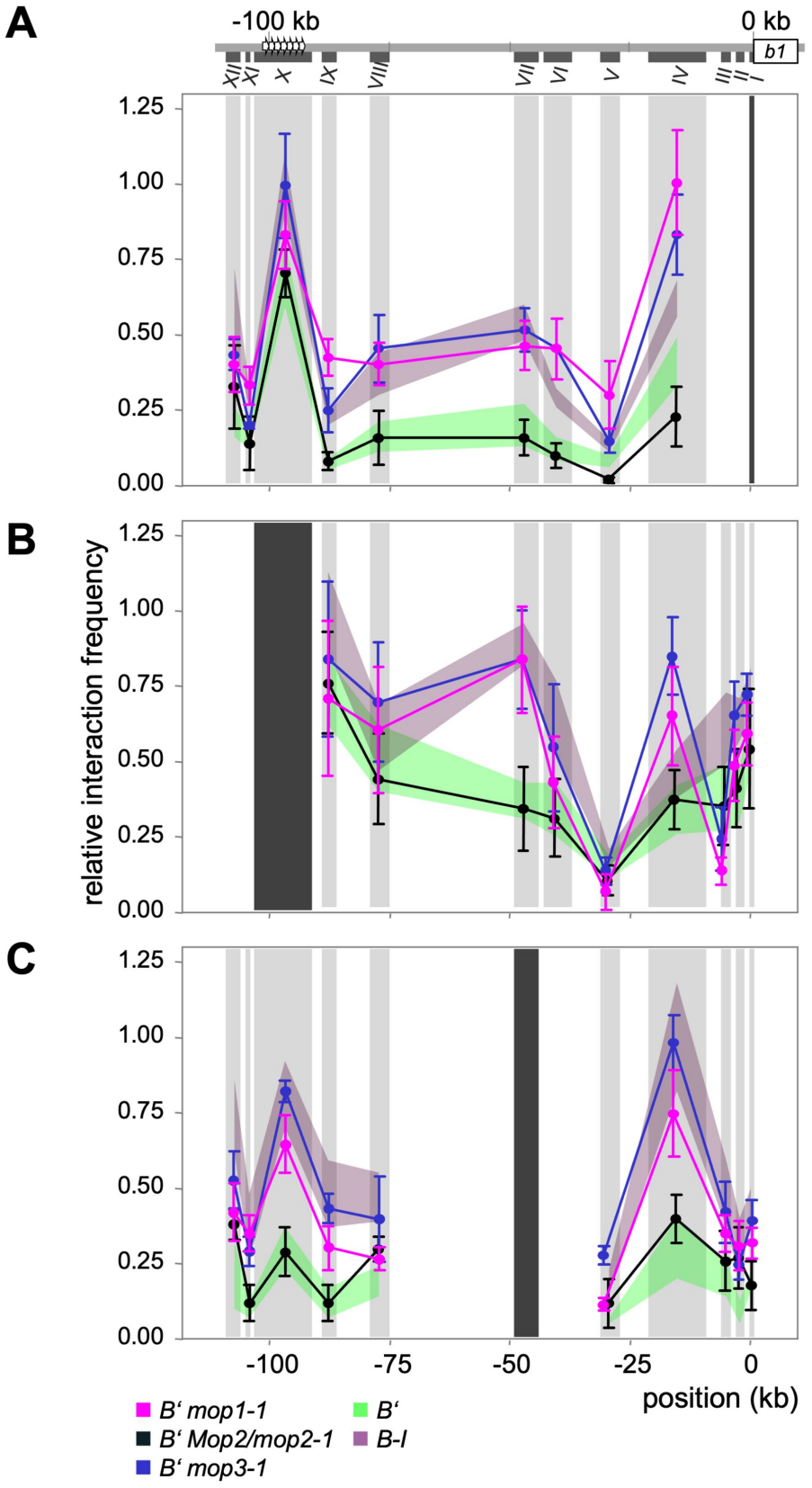

Figure 3. *B'* shows a multi-loop structure in the *mop1-1* and *mop3-1* mutant background, and a single loop structure in *Mop2/mop2-1* mutant background. At the top a schematic representation of the *b1* locus including the coding region (white box) and hepta-repeat enhancer (arrowheads). The *Bgl*II fragments (I-XII) examined by 3C are indicated as dark grey boxes. The viewpoints I (TSS; panel A), X (Hepta-repeat; panel B), and VII (~47kb upstream; panel C) are indicated by black vertical bars. Data were normalized using crosslinking frequencies measured for the *Sam* locus (Supplementary Figure S2). Error bars indicate the SEM of four biological replicates each for *B' mop1-1*, *B' Mop2/mop2-1* and *B' mop3-1*. Data for *B'* and *B-I* (reproduced from Louwers et al., 2009) are shown in shading for comparison. The experiments for *B'*, *B-I*, and the *mop* mutants were done in parallel.

Figure 4

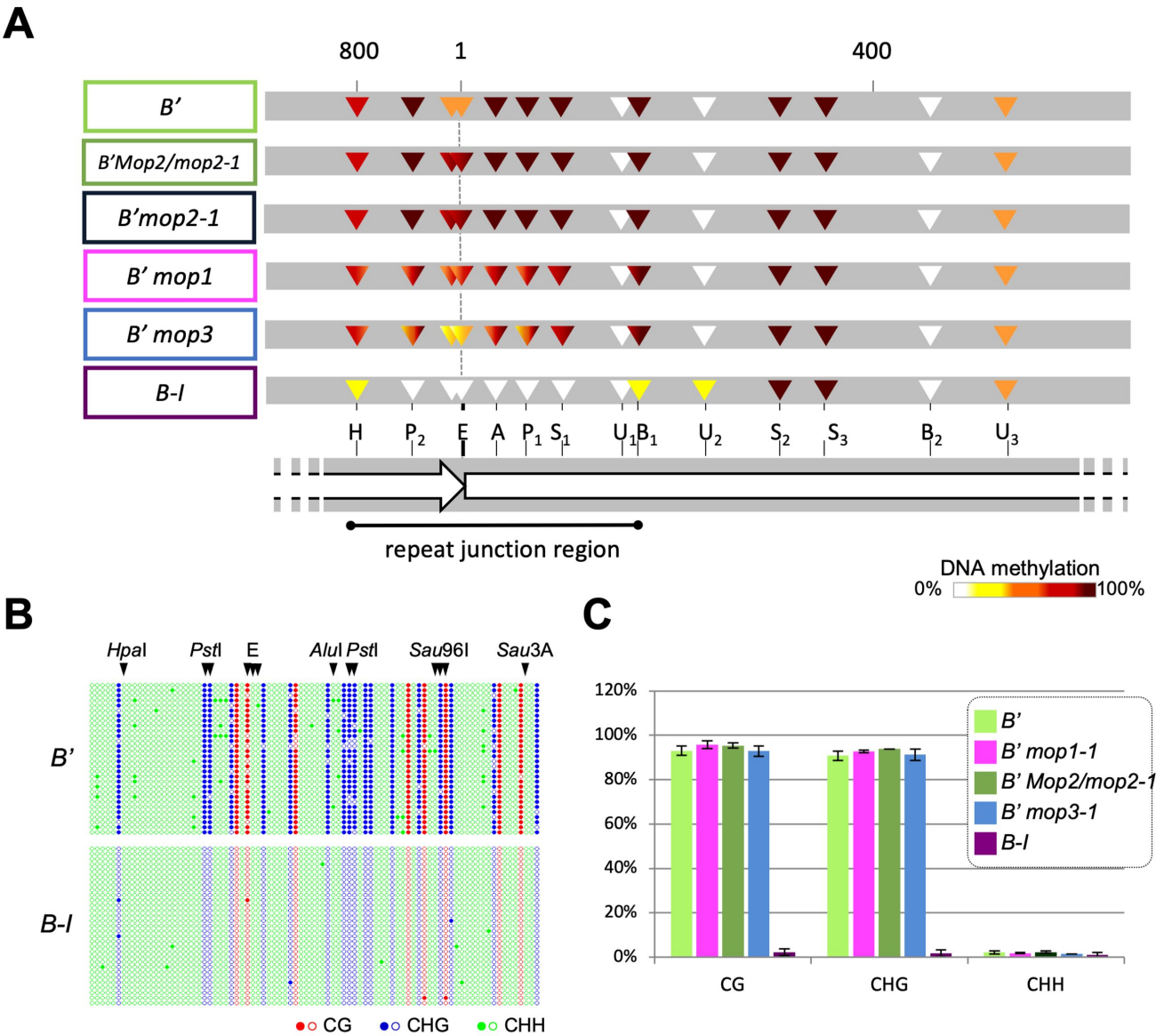

Figure 4. Differentially methylated repeat junction region retains high levels of symmetric DNA methylation in *mop* mutants. A) Summary of the DNA methylation levels data obtained by DNA blot analysis. DNA derived from *B'* wild type, *B-I* and *B' mop* mutants was digested with the methylation-insensitive *Eco*RI or *Bam*HI and the methylation-sensitive enzymes indicated. A zoom of part of the hepta-repeat, spanning the repeat junction region, is shown. The consensus repeat methylation profiles of *B'* and *B-I* (Haring et al., 2010) are shown. DNA methylation levels are specified by colors: 0-12.5%, white; 12.5-37.5%, yellow; 37.5-62.5%, orange; 62.5-87.5%, red; 87.5-100% methylation, dark red. H, *Hpa*I; P, *Pst*I; E, *Hha*I and *Hae*II; A, *Alu*I; S, *Sau*96I; U, *Sau*3AI; B, *Bsm*AI; Numbers discriminate individual sites present more than once every repeat. For details on the quantification of the DNA methylation levels see Haring *et al.* (2010). B) DNA methylation profiles of the *b1* repeat junction region at base-pair resolution for *B'* and *B-I*, generated by targeted bisulfite sequencing. This region includes the R1 and R6 loci assayed by ChIP-qPCR. See Supplementary Fig. S8 for all data sets. The dot-plots show the DNA methylation for 30 and 31 individual *B'* and *B-I* clones, respectively. Methylated and unmethylated cytosines are represented by filled and empty circles, respectively. Red, CG; Blue, CHG; Green, CHH. The restriction sites examined by DNA blotting are indicated above the panel for comparison. E indicates a site cut by both *Hha*I and *Hae*II. C) Total fraction of methylated cytosines in the repeat junction region in all three sequence contexts as measured by bisulfite sequencing. The mean and standard deviations shown are calculated from three (*B' mop1-1*) or two (all other genotypes) biological replicates. *M/mop2* indicates *Mop2/mop2-1*.

Figure 5

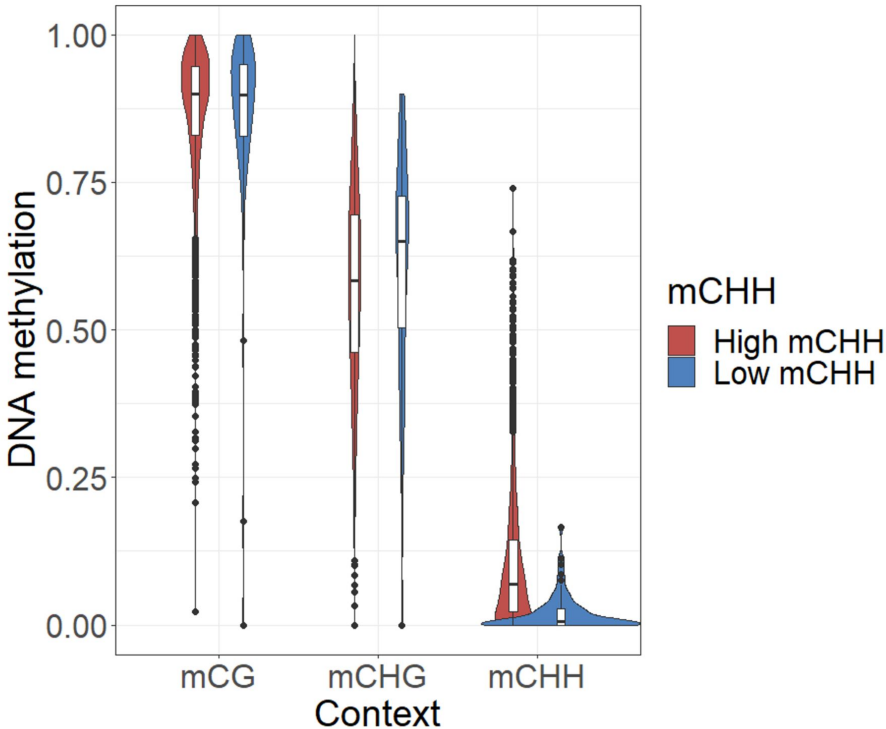

Figure 5. The maize genome contains low-mCHH and high-mCHH RdDM loci. Average DNA methylation levels for high and low mCHH loci in the developing second leaf of B73. Values of 5-methylcytosine are relative to the total number of cytosines (mC/total C) in each sequence context (CG, CHG, or CHH).

Figure 6

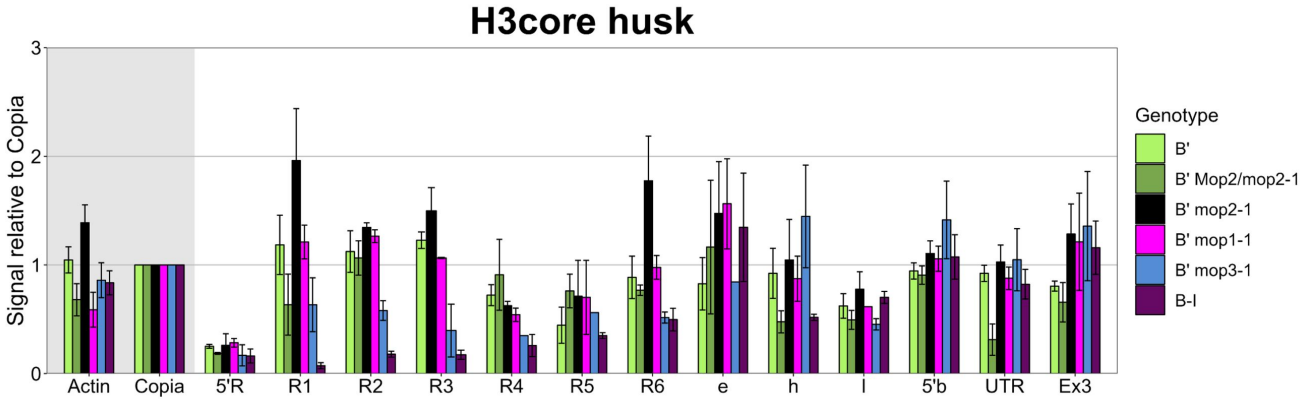

Figure 6. No significant decrease in nucleosome occupancy was observed in the *mop* mutants. ChIP experiments were performed with an antibody recognizing histone H3, using husk tissue from *B'* (light green), *B' Mop/mop2-1* (green), *B' mop2-1* (black), *B' mop1-1* (magenta), *B' mop3-1* (blue), and *B-I* (purple) plants. Data was normalized to *actin* values. The error bars indicate the standard error of the mean (SEM) of two (*B' mop1-1*), three (*B'*, *B' Mop/mop2-1*, *B' mop3-1),* or four (*B' mop2-1*, *B-I*) replicate experiments. For the no-antibody control signals see Supplemental Figure S10.

Figure 7

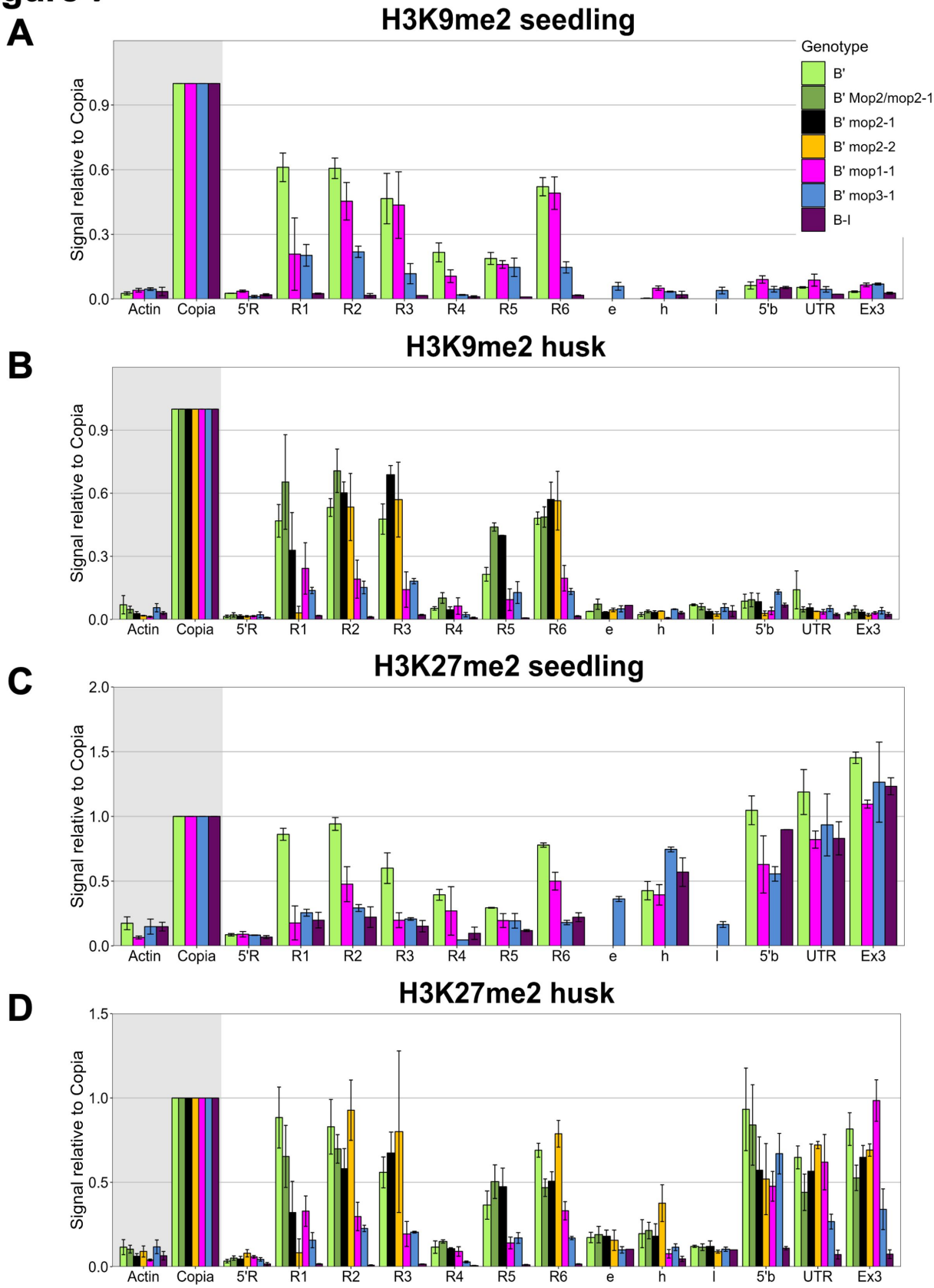

Figure 7. Transcriptional activation in *mop1-1* and *mop3-1* is associated with reduced levels of repressive histone marks. ChIP-qPCR experiments were performed on seedling (A, C) and husk tissue (B, D) from *B'*, *B' Mop/mop2-1*, *B' mop2-1*, *B' mop1-1*, *B' mop3-1* and *B-I* plants with antibodies recognizing H3K9me2 (A, B), and H3K27me2 (C, D). ChIP signals were normalized to *Copia* signals. Error bars indicate the SEM of multiple biological replicates. For seedlings, three (*B'*, *B' mop1-1*) or two (*B' mop3-1, B-I)* replicates were performed. For husks (B, D), two (*B' mop2-2*), three (*B', B' mop3-1*, *B-I*), or four (*B' mop1-1, B' Mop/mop2-1*, *B' mop2-1)* replicates were performed. For the no-antibody control signals see Supplemental Figure S11.

Parsed Citations

Alleman, M., Sidorenko, L., McGinnis, K., Seshadri, V., Dorweiler, J.E., White, J., Sikkink, K., Chandler, V.L., 2006. An RNA-dependent RNA polymerase is required for paramutation in maize. Nature 442, 295–298. https://doi.org/10.1038/nature04884
Google Scholar: Author Only Title Only Author and Title

Arteaga-Vazquez, M., Sidorenko, L., Rabanal, F.A., Shrivistava, R., Nobuta, K., Green, P.J., Meyers, B.C., Chandler, V.L., 2010. RNA-mediated trans -communication can establish paramutation at the b1 locus in maize. PNAS 107, 12986–12991. https://doi.org/10.1073/pnas.1007972107/-/DCSupplemental.www.pnas.org/cgi/doi/10.1073/pnas.1007972107
Google Scholar: Author Only Title Only Author and Title

Bartee, L., Malagnac, F., Bender, J., 2001. Arabidopsis cmt3 chromomethylase mutations block non-CG methylation and silencing of an endogenous gene. Genes Dev 15, 1753–1758. https://doi.org/10.1101/gad.905701
Google Scholar: Author Only Title Only Author and Title

Belele, C.L., Sidorenko, L., Stam, M., Bader, R., Arteaga-Vazquez, M.A., Chandler, V.L., 2013. Specific Tandem Repeats Are Sufficient for Paramutation-Induced Trans-Generational Silencing. PLoS Genetics 9. https://doi.org/10.1371/journal.pgen.1003773
Google Scholar: Author Only Title Only Author and Title

Bernatavichute, Y.V., Zhang, X., Cokus, S., Pellegrini, M., Jacobsen, S.E., 2008. Genome-wide association of histone H3 lysine nine methylation with CHG DNA methylation in Arabidopsis thaliana. PLoS One 3, e3156. https://doi.org/10.1371/journal.pone.0003156
Google Scholar: Author Only Title Only Author and Title

Calarco, J.P., Borges, F., Donoghue, M.T.A, Van Ex, F., Jullien, P.E., Lopes, T., Gardner, R., Berger, F., Feijó, J.A, Becker, J.D., Martienssen, R.A, 2012. Reprogramming of DNA Methylation in Pollen Guides Epigenetic Inheritance via Small RNA. Cell 151, 194–205. https://doi.org/10.1016/j.cell.2012.09.001
Google Scholar: Author Only Title Only Author and Title

Castel, S.E., Martienssen, R.A, 2013. RNA interference in the nucleus: roles for small RNAs in transcription, epigenetics and beyond. Nat Rev Genet 14, 100–112. https://doi.org/10.1038/nrg3355
Google Scholar: Author Only Title Only Author and Title

Conway, E., Healy, E., Bracken, A.P., 2015. PRC2 mediated H3K27 methylations in cellular identity and cancer. Curr Opin Cell Biol 37, 42–48. https://doi.org/10.1016/j.ceb.2015.10.003
Google Scholar: Author Only Title Only Author and Title

Dellaporta, S.L., Wood, J., Hicks, J.B., 1983. A plant DNA minipreparation: Version II. Plant Mol Biol Rep 1, 19–21. https://doi.org/10.1007/BF02712670
Google Scholar: Author Only Title Only Author and Title

Dorweiler, J.E., Carey, C.C., Kubo, K.M., Hollick, J.B., Kermicle, J.L., Chandler, V.L., 2000. mediator of paramutation1 is required for establishment and maintenance of paramutation at multiple maize loci. Plant Cell 12, 2101–2118. https://doi.org/10.1105/tpc.12.11.2101
Google Scholar: Author Only Title Only Author and Title

Du, J., Johnson, L.M., Groth, M., Feng, S., Hale, C.J., Li, S., Vashisht, A.A., Wohlschlegel, J.A., Patel, D.J., Jacobsen, S.E., 2014. Mechanism of DNA methylation-directed histone methylation by KRYPTONITE. Mol Cell 55, 495–504. https://doi.org/10.1016/j.molcel.2014.06.009
Google Scholar: Author Only Title Only Author and Title

Du, J., Zhong, X., Bernatavichute, Y.V., Stroud, H., Feng, S., Caro, E., Vashisht, A.A., Terragni, J., Chin, H.G., Tu, A., Hetzel, J., Wohlschlegel, J.A., Pradhan, S., Patel, D.J., Jacobsen, S.E., 2012. Dual binding of chromomethylase domains to H3K9me2-containing nucleosomes directs DNA methylation in plants. Cell 151, 167–180. https://doi.org/10.1016/j.cell.2012.07.034
Google Scholar: Author Only Title Only Author and Title

Egelhofer, T.A., Minoda, A., Klugman, S., Lee, K., Kolasinska-Zwierz, P., Alekseyenko, A.A., Cheung, M.-S., Day, D.S., Gadel, S., Gorchakov, A.A., Gu, T., Kharchenko, P.V., Kuan, S., Latorre, I., Linder-Basso, D., Luu, Y., Ngo, Q., Perry, M., Rechtsteiner, A., Riddle, N.C., Schwartz, Y.B., Shanower, G.A., Vielle, A., Ahringer, J., Elgin, S.C.R., Kuroda, M.I., Pirrotta, V., Ren, B., Strome, S., Park, P.J., Karpen, G.H., Hawkins, R.D., Lieb, J.D., 2011. An assessment of histone-modification antibody quality. Nat Struct Mol Biol 18, 91–93. https://doi.org/10.1038/nsmb.1972
Google Scholar: Author Only Title Only Author and Title

Erhard, K.F., Stonaker, J.L., Parkinson, S.E., Al., E., 2009. RNA Polymerase IV Functions in Paramutation in Zea mays. Science 323, 1201–1205.
Google Scholar: Author Only Title Only Author and Title

Ferrari, K.J., Scelfo, A., Jammula, S., Cuomo, A., Barozzi, I., Stützer, A., Fischle, W., Bonaldi, T., Pasini, D., 2014. Polycomb-dependent H3K27me1 and H3K27me2 regulate active transcription and enhancer fidelity. Mol Cell 53, 49–62. https://doi.org/10.1016/j.molcel.2013.10.030

Google Scholar: Author Only Title Only Author and Title

Fitz-James, M.H., Cavalli, G., 2022. Molecular mechanisms of transgenerational epigenetic inheritance. Nat Rev Genet 23, 325–341. https://doi.org/10.1038/s41576-021-00438-5
Google Scholar: Author Only Title Only Author and Title

Foda, B.M., Singh, U., 2015. Dimethylated H3K27 Is a Repressive Epigenetic Histone Mark in the Protist Entamoeba histolytica and Is Significantly Enriched in Genes Silenced via the RNAi Pathway. Journal of Biological Chemistry 290, 21114–21130. https://doi.org/10.1074/jbc.M115.647263
Google Scholar: Author Only Title Only Author and Title

Fu, F.-F., Dawe, R.K., Gent, J.I., 2018. Loss of RNA-Directed DNA Methylation in Maize Chromomethylase and DDM1-Type Nucleosome Remodeler Mutants. The Plant Cell 30, 1617–1627. https://doi.org/10.1105/tpc.18.00053
Google Scholar: Author Only Title Only Author and Title

Gent, Jonathan I, Ellis, N.A, Guo, L., Harkess, A.E., Yao, Y., Zhang, X., Dawe, R.K., 2013. CHH islands : de novo DNA methylation in near-gene chromatin regulation in maize. Genome research 23, 628–637. https://doi.org/10.1101/gr.146985.112.as
Google Scholar: Author Only Title Only Author and Title

Gent, J I, Ellis, N.A, Guo, L., Harkess, A.E., Yao, Y., Zhang, X., Dawe, R.K., 2013. CHH islands: de novo DNA methylation in near-gene chromatin regulation in maize. Genome Research 23, 628–637. https://doi.org/10.1101/gr.146985.112
Google Scholar: Author Only Title Only Author and Title

Gent, J.I., Higgins, K.M., Swentowsky, K.W., Fu, F.-F., Zeng, Y., Kim, D.W., Dawe, R.K., Springer, N.M., Anderson, S.N., 2022. The maize gene maternal derepression of r1 encodes a DNA glycosylase that demethylates DNA and reduces siRNA expression in the endosperm. Plant Cell 34, 3685–3701. https://doi.org/10.1093/plcell/koac199
Google Scholar: Author Only Title Only Author and Title

Gent, Jonathan I, Madzima, T.F., Bader, R., Kent, M.R., Zhang, X., Stam, M., McGinnis, K.M., Dawe, R.K., 2014b. Accessible DNA and Relative Depletion of H3K9me2 at Maize Loci Undergoing RNA-Directed DNA Methylation. The Plant Cell Online 26, 4903–4917. https://doi.org/10.1105/tpc.114.130427
Google Scholar: Author Only Title Only Author and Title

Grewal, S.I.S., 2023. The molecular basis of heterochromatin assembly and epigenetic inheritance. Mol Cell 83, 1767–1785. https://doi.org/10.1016/j.molcel.2023.04.020
Google Scholar: Author Only Title Only Author and Title

Gruntman, E., Qi, Y., Slotkin, R.K., Roeder, T., Martienssen, R.A., Sachidanandam, R., 2008. Kismeth: Analyzer of plant methylation states through bisulfite sequencing. BMC Bioinformatics 9, 371. https://doi.org/10.1186/1471-2105-9-371
Google Scholar: Author Only Title Only Author and Title

Gu, S.G., Pak, J., Guang, S., Maniar, J.M., Kennedy, S., Fire, A., 2012. Amplification of siRNA in Caenorhabditis elegans generates a transgenerational sequence-targeted histone H3 lysine 9 methylation footprint. Nat Genet 44, 157–164. https://doi.org/10.1038/ng.1039
Google Scholar: Author Only Title Only Author and Title

Guo, W., Fiziev, P., Yan, W., Cokus, S., Sun, X., Zhang, M.Q., Chen, P.Y., Pellegrini, M., 2013. BS-Seeker2: A versatile aligning pipeline for bisulfite sequencing data. BMC Genomics 14, 1. https://doi.org/10.1186/1471-2164-14-774
Google Scholar: Author Only Title Only Author and Title

Guo, W., Zhu, P., Pellegrini, M., Zhang, M.Q., Wang, X., Ni, Z., 2018. CGmapTools improves the precision of heterozygous SNV calls and supports allele-specific methylation detection and visualization in bisulfite-sequencing data. Bioinformatics 34, 381–387. https://doi.org/10.1093/bioinformatics/btx595
Google Scholar: Author Only Title Only Author and Title

Gutiérrez-Marcos, J.F., Costa, L.M., Dal Prà, M., Scholten, S., Kranz, E., Perez, P., Dickinson, H.G., 2006. Epigenetic asymmetry of imprinted genes in plant gametes. Nat Genet 38, 876–878. https://doi.org/10.1038/ng1828
Google Scholar: Author Only Title Only Author and Title

Haag, J.R., Brower-Toland, B., Krieger, E.K., Sidorenko, L., Nicora, C.D., Norbeck, A.D., Irsigler, A., LaRue, H., Brzeski, J., McGinnis, K., Ivashuta, S., Pasa-Tolic, L., Chandler, V.L., Pikaard, C.S., 2014. Functional diversification of maize RNA polymerase IV and V subtypes via alternative catalytic subunits. Cell reports 9, 378–90. https://doi.org/10.1016/j.celrep.2014.08.067
Google Scholar: Author Only Title Only Author and Title

Haring, M., Bader, R., Louwers, M., Schwabe, A., van Driel, R., Stam, M., 2010a. The role of DNA methylation, nucleosome occupancy and histone modifications in paramutation. The Plant journal : for cell and molecular biology 63, 366–78. https://doi.org/10.1111/j.1365-313X.2010.04245.x
Google Scholar: Author Only Title Only Author and Title

Haring, M., Offermann, S., Danker, T., Horst, I., Peterhansel, C., Stam, M., 2007. Chromatin immunoprecipitation: optimization,

quantitative analysis and data normalization. Plant Methods 3, 11. https://doi.org/10.1186/1746-4811-3-11
Google Scholar: Author Only Title Only Author and Title

Herr, A.J., Jensen, M.B., Dalmay, T., Baulcombe, D.C., 2005. RNA polymerase IV directs silencing of endogenous DNA. Science 308, 118–120. https://doi.org/10.1126/science.1106910
Google Scholar: Author Only Title Only Author and Title

Hollick, J.B., 2017. Paramutation and related phenomena in diverse species. Nat Rev Genet 18, 5–23. https://doi.org/10.1038/nrg.2016.115
Google Scholar: Author Only Title Only Author and Title

Hollick, Jay B, Kermicle, J.L., Parkinson, S.E., 2005. Rmr6 maintains meiotic inheritance of paramutant states in Zea mays. Genetics 171, 725–40. https://doi.org/10.1534/genetics.105.045260
Google Scholar: Author Only Title Only Author and Title

Hollick, J. B., Kermicle, J.L., Parkinson, S.E., 2005. Rmr6 maintains meiotic inheritance of paramutant states in Zea mays. Genetics 171, 725–740. https://doi.org/10.1534/genetics.105.045260
Google Scholar: Author Only Title Only Author and Title

Hollick, J.B., Patterson, G.I., Coe, E.H., Cone, J.K.C., Chandler, V.L., 1995. Allelic Interactions Heritably Alter the Activity of a Metastable Maize pl Allele. Genetics 141, 709–719.
Google Scholar: Author Only Title Only Author and Title

Hövel, I., Pearson, N.A., Stam, M., 2015. Cis-acting determinants of paramutation. Semin Cell Dev Biol 44, 22–32. https://doi.org/10.1016/j.semcdb.2015.08.012
Google Scholar: Author Only Title Only Author and Title

Hufford, M.B., Seetharam, A.S., Woodhouse, M.R., Chougule, K.M., Ou, S., Liu, J., Ricci, W.A., Guo, T., Olson, A., Qiu, Y., Della Coletta, R., Tittes, S., Hudson, A.I., Marand, A.P., Wei, S., Lu, Z., Wang, B., Tello-Ruiz, M.K., Piri, R.D., Wang, N., Kim, D.W., Zeng, Y., O'Connor, C.H., Li, X., Gilbert, A.M., Baggs, E., Krasileva, K.V., Portwood, J.L., Cannon, E.K.S., Andorf, C.M., Manchanda, N., Snodgrass, S.J., Hufnagel, D.E., Jiang, Q., Pedersen, S., Syring, M.L., Kudrna, D.A., Llaca, V., Fengler, K., Schmitz, R.J., Ross-Ibarra, J., Yu, J., Gent, J.I., Hirsch, C.N., Ware, D., Dawe, R.K., 2021. De novo assembly, annotation, and comparative analysis of 26 diverse maize genomes. Science 373, 655–662. https://doi.org/10.1126/science.abg5289
Google Scholar: Author Only Title Only Author and Title

Jackel, J.N., Storer, J.M., Coursey, T., Bisaro, D.M., 2016. Arabidopsis RNA Polymerases IV and V Are Required To Establish H3K9 Methylation, but Not Cytosine Methylation, on Geminivirus Chromatin. Journal of Virology 90, 7529–7540. https://doi.org/10.1128/jvi.00656-16
Google Scholar: Author Only Title Only Author and Title

Jia, Y., Lisch, D.R., Ohtsu, K., Scanlon, M.J., Nettleton, D., Schnable, P.S., 2009. Loss of RNA-dependent RNA polymerase 2 (RDR2) function causes widespread and unexpected changes in the expression of transposons, genes, and 24-nt small RNAs. PLoS Genet 5, e1000737. https://doi.org/10.1371/journal.pgen.1000737
Google Scholar: Author Only Title Only Author and Title

Jiang, C., Pugh, B.F., 2009. Nucleosome positioning and gene regulation: advances through genomics. Nat Rev Genet 10, 161–172. https://doi.org/10.1038/nrg2522
Google Scholar: Author Only Title Only Author and Title

Johnson, L.M., Bostick, M., Zhang, X., Kraft, E., Henderson, I., Callis, J., Jacobsen, S.E., 2007. The SRA methyl-cytosine-binding domain links DNA and histone methylation. Curr Biol 17, 379–384. https://doi.org/10.1016/j.cub.2007.01.009
Google Scholar: Author Only Title Only Author and Title

Kanno, T., Huettel, B., Mette, M.F., Aufsatz, W., Jaligot, E., Daxinger, L., Kreil, D.P., Matzke, M., Matzke, A.J.M., 2005. Atypical RNA polymerase subunits required for RNA-directed DNA methylation. Nat Genet 37, 761–765. https://doi.org/10.1038/ng1580
Google Scholar: Author Only Title Only Author and Title

Langmead, B., Salzberg, S.L., 2012. Fast gapped-read alignment with Bowtie 2. Nat Methods 9, 357–359. https://doi.org/10.1038/nmeth.1923
Google Scholar: Author Only Title Only Author and Title

Law, J.A., Vashisht, A.A., Wohlschlegel, J.A., Jacobsen, S.E., 2011. SHH1, a homeodomain protein required for DNA methylation, as well as RDR2, RDM4, and chromatin remodeling factors, associate with RNA polymerase IV. PLoS Genet 7, e1002195. https://doi.org/10.1371/journal.pgen.1002195
Google Scholar: Author Only Title Only Author and Title

Lee, H.-G., Kahn, T.G., Simcox, A., Schwartz, Y.B., Pirrotta, V., 2015. Genome-wide activities of Polycomb complexes control pervasive transcription. Genome Res. 25, 1170–1181. https://doi.org/10.1101/gr.188920.114
Google Scholar: Author Only Title Only Author and Title

Li, H., Handsaker, B., Wysoker, A., Fennell, T., Ruan, J., Homer, N., Marth, G., Abecasis, G., Durbin, R., 1000 Genome Project Data Processing Subgroup, 2009. The Sequence Alignment/Map format and SAMtools. Bioinformatics 25, 2078–2079. https://doi.org/10.1093/bioinformatics/btp352
Google Scholar: Author Only Title Only Author and Title

Li, Q., Eichten, S.R., Hermanson, P.J., Zaunbrecher, V.M., Song, J., Wendt, J., Rosenbaum, H., Madzima, T.F., Sloan, A.E., Huang, J., Burgess, D.L., Richmond, T.A., McGinnis, K.M., Meeley, R.B., Danilevskaya, O.N., Vaughn, M.W., Kaeppler, S.M., Jeddeloh, J.A., Springer, N.M., 2014. Genetic Perturbation of the Maize Methylome. The Plant Cell Online 26, 4602–4616. https://doi.org/10.1105/tpc.114.133140
Google Scholar: Author Only Title Only Author and Title

Li, Q., Gent, J.I., Zynda, G., Song, J., Makarevitch, I., Hirsch, C.D., Hirsch, C.N., Dawe, R.K., Madzima, T.F., McGinnis, K.M., Lisch, D., Schmitz, R.J., Vaughn, M.W., Springer, N.M., 2015. RNA-directed DNA methylation enforces boundaries between heterochromatin and euchromatin in the maize genome. Proceedings of the National Academy of Sciences 112, 14728–14733. https://doi.org/10.1073/pnas.1514680112
Google Scholar: Author Only Title Only Author and Title

Lindroth, A.M., Cao, X., Jackson, J.P., Zilberman, D., McCallum, C.M., Henikoff, S., Jacobsen, S.E., 2001. Requirement of CHROMOMETHYLASE3 for maintenance of CpXpG methylation. Science 292, 2077–2080. https://doi.org/10.1126/science.1059745
Google Scholar: Author Only Title Only Author and Title

Liu, Y., Taverna, S.D., Muratore, T.L., Shabanowitz, J., Hunt, D.F., Allis, C.D., 2007. RNAi-dependent H3K27 methylation is required for heterochromatin formation and DNA elimination in Tetrahymena. Genes Dev 21, 1530–1545. https://doi.org/10.1101/gad.1544207
Google Scholar: Author Only Title Only Author and Title

Liu, Y., Yuan, J., Jia, G., Ye, W., Jeffrey Chen, Z., Song, Q., 2021. Histone H3K27 dimethylation landscapes contribute to genome stability and genetic recombination during wheat polyploidization. The Plant Journal 105, 678–690. https://doi.org/10.1111/tpj.15063
Google Scholar: Author Only Title Only Author and Title

Locatelli, S., Piatti, P., Motto, M., Rossi, V., 2009. Chromatin and DNA modifications in the Opaque2-mediated regulation of gene transcription during maize endosperm development. Plant Cell 21, 1410–1427. https://doi.org/10.1105/tpc.109.067256
Google Scholar: Author Only Title Only Author and Title

Louwers, M., Bader, R., Haring, M., van Driel, R., de Laat, W., Stam, M., 2009a. Tissue- and expression level-specific chromatin looping at maize b1 epialleles. The Plant Cell 21, 832–42. https://doi.org/10.1105/tpc.108.064329
Google Scholar: Author Only Title Only Author and Title

Louwers, M., Splinter, E., van Driel, R., de Laat, W., Stam, M., 2009b. Studying physical chromatin interactions in plants using Chromosome Conformation Capture (3C). Nat Protoc 4, 1216–1229. https://doi.org/10.1038/nprot.2009.113
Google Scholar: Author Only Title Only Author and Title

Martin, M., 2011. Cutadapt removes adapter sequences from high-throughput sequencing reads. EMBnet.journal 17, 10–12. https://doi.org/10.14806/ej.17.1.200
Google Scholar: Author Only Title Only Author and Title

Mathieu, O., Probst, A.V., Paszkowski, J., 2005. Distinct regulation of histone H3 methylation at lysines 27 and 9 by CpG methylation in Arabidopsis. The EMBO Journal 24, 2783–2791. https://doi.org/10.1038/sj.emboj.7600743
Google Scholar: Author Only Title Only Author and Title

Mathieu, O., Reinders, J., Caikovski, M., Smathajitt, C., Paszkowski, J., 2007. Transgenerational stability of the Arabidopsis epigenome is coordinated by CG methylation. Cell 130, 851–862. https://doi.org/10.1016/j.cell.2007.07.007
Google Scholar: Author Only Title Only Author and Title

Matzke, M.A., Mosher, R.A., 2014. RNA-directed DNA methylation: an epigenetic pathway of increasing complexity. Nat Rev Genet 15, 394–408. https://doi.org/10.1038/nrg3683
Google Scholar: Author Only Title Only Author and Title

Mishra, V., Singh, J., Wang, F., Zhang, Y., Fukudome, A., Trinidad, J.C., Takagi, Y., Pikaard, C.S., 2021. Assembly of a dsRNA synthesizing complex: RNA-DEPENDENT RNA POLYMERASE 2 contacts the largest subunit of NUCLEAR RNA POLYMERASE IV. Proc Natl Acad Sci U S A 118, e2019276118. https://doi.org/10.1073/pnas.2019276118
Google Scholar: Author Only Title Only Author and Title

Nobuta, K., Lu, C., Shrivastava, R., Pillay, M., De Paoli, E., Accerbi, M., Arteaga-Vazquez, M., Sidorenko, L., Jeong, D.-H., Yen, Y., Green, P.J., Chandler, V.L., Meyers, B.C., 2008a. Distinct size distribution of endogeneous siRNAs in maize: Evidence from deep sequencing in the mop1-1 mutant. Proc Natl Acad Sci U S A 105, 14958–14963. https://doi.org/10.1073/pnas.0808066105
Google Scholar: Author Only Title Only Author and Title

Nobuta, K., Lu, C., Shrivastava, R., Pillay, M., Paoli, E. De, Accerbi, M., Arteaga-vazquez, M., Sidorenko, L., Jeong, D., Yen, Y.,

Green, P.J., Chandler, V.L., Meyers, B.C., 2008b. Distinct size distribution of endogenous siRNAs in maize : Evidence from deep sequencing in the mop1-1 mutant. PNAS 105, 14958–14963.
Google Scholar: Author Only Title Only Author and Title

Ohtsu, K., Smith, M.B., Emrich, S.J., Borsuk, L.A., Zhou, R., Chen, T., Zhang, X., Timmermans, M.C.P., Beck, J., Buckner, B., Janick-Buckner, D., Nettleton, D., Scanlon, M.J., Schnable, P.S., 2007. Global gene expression analysis of the shoot apical meristem of maize (Zea mays L.). Plant J 52, 391–404. https://doi.org/10.1111/j.1365-313X.2007.03244.x
Google Scholar: Author Only Title Only Author and Title

Onodera, Y., Haag, J.R., Ream, T., Costa Nunes, P., Pontes, O., Pikaard, C.S., 2005. Plant nuclear RNA polymerase IV mediates siRNA and DNA methylation-dependent heterochromatin formation. Cell 120, 613–622. https://doi.org/10.1016/j.cell.2005.02.007
Google Scholar: Author Only Title Only Author and Title

Pal-Bhadra, M., Leibovitch, B.A., Gandhi, S.G., Rao, M., Bhadra, U., Birchler, J.A., Elgin, S.C.R., 2004. Heterochromatic Silencing and HP1 Localization in Drosophila Are Dependent on the RNAi Machinery. Science 303, 669–672. https://doi.org/10.1126/science.1092653
Google Scholar: Author Only Title Only Author and Title

Papa, C.M., Springer, N.M., Muszynski, M.G., Meeley, R., Kaeppler, S.M., 2001. Maize chromomethylase Zea methyltransferase2 is required for CpNpG methylation. Plant Cell 13, 1919–1928. https://doi.org/10.1105/tpc.010064
Google Scholar: Author Only Title Only Author and Title

Parent, J.-S., Cahn, J., Herridge, R.P., Grimanelli, D., Martienssen, R.A., 2021. Small RNAs guide histone methylation in Arabidopsis embryos. Genes Dev. 35, 841–846. https://doi.org/10.1101/gad.343871.120
Google Scholar: Author Only Title Only Author and Title

Park, S., Oh, S., Nocker, S. van, 2012. Genomic and Gene-Level Distribution of Histone H3 Dimethyl Lysine-27 (H3K27me2) in Arabidopsis. PLOS ONE 7, e52855. https://doi.org/10.1371/journal.pone.0052855
Google Scholar: Author Only Title Only Author and Title

Patterson, G.I., Thorpe, C.J., Chandler, V.L., 1993. Paramutation, an allelic interaction, is associated with a stable and heritable reduction of transcription of the maize b regulatory gene. Genetics 135, 881–894. https://doi.org/10.1093/genetics/135.3.881
Google Scholar: Author Only Title Only Author and Title

Plank, J.L., Dean, A., 2014. Enhancer function: mechanistic and genome-wide insights come together. Mol Cell 55, 5–14. https://doi.org/10.1016/j.molcel.2014.06.015
Google Scholar: Author Only Title Only Author and Title

Pontier, D., Yahubyan, G., Vega, D., Bulski, A., Saez-Vasquez, J., Hakimi, M.-A., Lerbs-Mache, S., Colot, V., Lagrange, T., 2005. Reinforcement of silencing at transposons and highly repeated sequences requires the concerted action of two distinct RNA polymerases IV in Arabidopsis. Genes Dev 19, 2030–2040. https://doi.org/10.1101/gad.348405
Google Scholar: Author Only Title Only Author and Title

Quinlan, A.R., Hall, I.M., 2010. BEDTools: a flexible suite of utilities for comparing genomic features. Bioinformatics 26, 841–842. https://doi.org/10.1093/bioinformatics/btq033
Google Scholar: Author Only Title Only Author and Title

Ritchie, S.W., Hanway, J.J., Benson, G.O., 1986. How a corn plant develops, 1986 (Departmental Report).

Ronsseray, S., 2015. Paramutation phenomena in non-vertebrate animals. Semin Cell Dev Biol 44, 39–46. https://doi.org/10.1016/j.semcdb.2015.08.009
Google Scholar: Author Only Title Only Author and Title

Roudier, F., Ahmed, I., Bérard, C., Sarazin, A., Mary-Huard, T., Cortijo, S., Bouyer, D., Caillieux, E., Duvernois-Berthet, E., Al-Shikhley, L., Giraut, L., Després, B., Drevensek, S., Barneche, F., Dèrozier, S., Brunaud, V., Aubourg, S., Schnittger, A., Bowler, C., Martin-Magniette, M.-L., Robin, S., Caboche, M., Colot, V., 2011. Integrative epigenomic mapping defines four main chromatin states in Arabidopsis: Organization of the Arabidopsis epigenome. The EMBO Journal 30, 1928–1938. https://doi.org/10.1038/emboj.2011.103
Google Scholar: Author Only Title Only Author and Title

Rymen, B., Ferrafiat, L., Blevins, T., 2020. Non-coding RNA polymerases that silence transposable elements and reprogram gene expression in plants. Transcription 11, 172–191. https://doi.org/10.1080/21541264.2020.1825906
Google Scholar: Author Only Title Only Author and Title

Schmitz, R.J., Grotewold, E., Stam, M., 2022. Cis-regulatory sequences in plants: Their importance, discovery, and future challenges. Plant Cell 34, 718–741. https://doi.org/10.1093/plcell/koab281
Google Scholar: Author Only Title Only Author and Title

Sekhon, R.S., Lin, H., Childs, K.L., Hansey, C.N., Buell, C.R., de Leon, N., Kaeppler, S.M., 2011. Genome-wide atlas of transcription during maize development. Plant J 66, 553–563. https://doi.org/10.1111/j.1365-313X.2011.04527.x

Google Scholar: Author Only Title Only Author and Title

Sekhon, R.S., Wang, P.-H., Sidorenko, L., Chandler, V.L., Chopra, S., 2012. Maize Unstable factor for orange1 is required for maintaining silencing associated with paramutation at the pericarp color1 and booster1 loci. PLoS Genet 8, e1002980. https://doi.org/10.1371/journal.pgen.1002980
Google Scholar: Author Only Title Only Author and Title

Sidorenko, L., Chandler, V., 2008. RNA-dependent RNA polymerase is required for enhancer-mediated transcriptional silencing associated with paramutation at the maize p1 gene. Genetics 180, 1983–1993. https://doi.org/10.1534/genetics.108.095281
Google Scholar: Author Only Title Only Author and Title

Sidorenko, L., Dorweiler, J.E., Cigan, a M., Arteaga-Vazquez, M., Vyas, M., Kermicle, J., Jurcin, D., Brzeski, J., Cai, Y., Chandler, V.L., 2009. A dominant mutation in mediator of paramutation2, one of three second-largest subunits of a plant-specific RNA polymerase, disrupts multiple siRNA silencing processes. PLoS genetics 5, e1000725. https://doi.org/10.1371/journal.pgen.1000725
Google Scholar: Author Only Title Only Author and Title

Sloan, Amy E., Sidorenko, L., McGinnis, K.M., 2014. Diverse gene-silencing mechanisms with distinct requirements for RNA polymerase subunits in Zea mays. Genetics 198, 1031–1042. https://doi.org/10.1534/genetics.114.168518
Google Scholar: Author Only Title Only Author and Title

Springer, N.M., McGinnis, K.M., 2015. Paramutation in evolution, population genetics and breeding. Semin Cell Dev Biol 44, 33–38. https://doi.org/10.1016/j.semcdb.2015.08.010
Google Scholar: Author Only Title Only Author and Title

Stam, M., Belele, C., Dorweiler, J.E., Chandler, V.L., 2002a. Differential chromatin structure within a tandem array 100 kb upstream of the maize b1 locus is associated with paramutation. Genes and Development 16, 1906–1918. https://doi.org/10.1101/gad.1006702
Google Scholar: Author Only Title Only Author and Title

Stam, M., Belele, C., Ramakrishna, W., Dorweiler, J.E., Bennetzen, J.L., Chandler, V.L., 2002b. The regulatory regions required for B' paramutation and expression are located far upstream of the maize b1 transcribed sequences. Genetics 162, 917–930. https://doi.org/10.1093/genetics/162.2.917
Google Scholar: Author Only Title Only Author and Title

Stonaker, Jennifer L., Lim, J.P., Erhard, K.F., Hollick, J.B., 2009. Diversity of Pol IV function is defined by mutations at the maize rmr7 locus. PLoS Genet 5, e1000706. https://doi.org/10.1371/journal.pgen.1000706
Google Scholar: Author Only Title Only Author and Title

Stroud, H., Do, T., Du, J., Zhong, X., Feng, S., Johnson, L., Patel, D.J., Jacobsen, S.E., 2014. Non-CG methylation patterns shape the epigenetic landscape in Arabidopsis. Nat Struct Mol Biol 21, 64–72. https://doi.org/10.1038/nsmb.2735
Google Scholar: Author Only Title Only Author and Title

Stroud, H., Greenberg, M.V.C., Feng, S., Bernatavichute, Y.V., Jacobsen, S.E., 2013. Comprehensive analysis of silencing mutants reveals complex regulation of the Arabidopsis methylome. Cell 152, 352–364. https://doi.org/10.1016/j.cell.2012.10.054
Google Scholar: Author Only Title Only Author and Title

Struhl, K., Segal, E., 2013. Determinants of nucleosome positioning. Nat Struct Mol Biol 20, 267–273. https://doi.org/10.1038/nsmb.2506
Google Scholar: Author Only Title Only Author and Title

Tang, K., Lang, Z., Zhang, H., Zhu, J.-K., 2016. The DNA demethylase ROS1 targets genomic regions with distinct chromatin modifications. Nat Plants 2, 16169. https://doi.org/10.1038/nplants.2016.169
Google Scholar: Author Only Title Only Author and Title

Underwood, C.J., Choi, K., Lambing, C., Zhao, X., Serra, H., Borges, F., Simorowski, J., Ernst, E., Jacob, Y., Henderson, I.R., Martienssen, R.A., 2018. Epigenetic activation of meiotic recombination near Arabidopsis thaliana centromeres via loss of H3K9me2 and non-CG DNA methylation. Genome Res 28, 519–531. https://doi.org/10.1101/gr.227116.117
Google Scholar: Author Only Title Only Author and Title

Verdel, A., Jia, S., Gerber, S., Sugiyama, T., Gygi, S., Grewal, S.I.S., Moazed, D., 2004. RNAi-mediated targeting of heterochromatin by the RITS complex. Science 303, 672–676. https://doi.org/10.1126/science.1093686
Google Scholar: Author Only Title Only Author and Title

West, P.T., Li, Q., Ji, L., Eichten, S.R., Song, J., Vaughn, M.W., Schmitz, R.J., Springer, N.M., 2014. Genomic distribution of H3K9me2 and DNA methylation in a maize genome. PLoS One 9, e105267. https://doi.org/10.1371/journal.pone.0105267
Google Scholar: Author Only Title Only Author and Title

Wierzbicki, A.T., Haag, J.R., Pikaard, C.S., 2008. Noncoding transcription by RNA polymerase Pol IVb/Pol V mediates transcriptional silencing of overlapping and adjacent genes. Cell 135, 635–648. https://doi.org/10.1016/j.cell.2008.09.035

Google Scholar: Author Only Title Only Author and Title

Woodhouse, M.R., Freeling, M., Lisch, D., 2006a. Initiation, establishment, and maintenance of heritable MuDR transposon silencing in maize are mediated by distinct factors. PLoS Biol 4, e339. https://doi.org/10.1371/journal.pbio.0040339
Google Scholar: Author Only Title Only Author and Title

Woodhouse, M.R., Freeling, M., Lisch, D., 2006b. The mop1 (mediator of paramutation1) mutant progressively reactivates one of the two genes encoded by the MuDR transposon in maize. Genetics 172, 579–592. https://doi.org/10.1534/genetics.105.051383
Google Scholar: Author Only Title Only Author and Title

Xie, W., Schultz, M.D., Lister, R., Hou, Z., Rajagopal, N., Ray, P., Whitaker, J.W., Tian, S., Hawkins, R.D., Leung, D., Yang, H., Wang, T., Lee, A.Y., Swanson, S.A., Zhang, J., Zhu, Y., Kim, A., Nery, J.R., Urich, M.A., Kuan, S., Yen, C., Klugman, S., Yu, P., Suknuntha, K., Propson, N.E., Chen, H., Edsall, L.E., Wagner, U., Li, Y., Ye, Z., Kulkarni, A., Xuan, Z., Chung, W.-Y., Chi, N.C., Antosiewicz-Bourget, J.E., Slukvin, I., Stewart, R., Zhang, M.Q., Wang, W., Thomson, J.A., Ecker, J.R., Ren, B., 2013. Epigenomic analysis of multilineage differentiation of human embryonic stem cells. Cell 153, 1134–1148. https://doi.org/10.1016/j.cell.2013.04.022
Google Scholar: Author Only Title Only Author and Title

Zemach, A., Kim, M.Y., Hsieh, P.-H., Coleman-Derr, D., Eshed-Williams, L., Thao, K., Harmer, S.L., Zilberman, D., 2013. The Arabidopsis Nucleosome Remodeler DDM1 Allows DNA Methyltransferases to Access H1-Containing Heterochromatin. Cell 153, 193–205. https://doi.org/10.1016/j.cell.2013.02.033
Google Scholar: Author Only Title Only Author and Title

Zofall, M., Sandhu, R., Holla, S., Wheeler, D., Grewal, S.I.S., 2022. Histone deacetylation primes self-propagation of heterochromatin domains to promote epigenetic inheritance. Nat Struct Mol Biol 29, 898–909. https://doi.org/10.1038/s41594-022-00830-7
Google Scholar: Author Only Title Only Author and Title